






RESEARCH ARTICLE



Hidden in plain sight: A microanalytical study of a Middle Stone Age ochre piece trapped inside a micromorphological block sample

Magnus M. Haaland^{1,2,3}  | André M. Strauss⁴  | Elizabeth C. Velliky^{1,2}  |
 Susan M. Mentzer^{3,5} | Christopher E. Miller^{2,3,5} | Karen L. van Niekerk^{1,2}  |
 Christopher S. Henshilwood^{1,2,6} 

¹Department of Archaeology, History, Cultural Studies and Religion, University of Bergen, Bergen, Norway

²Centre for Early Sapiens Behaviour (SapienCE), University of Bergen, Bergen, Norway

³Institute for Archaeological Sciences, University of Tübingen, Tübingen, Germany

⁴Museu de Arqueologia e Etnologia, Universidade de São Paulo, São Paulo, São Paulo, Brazil

⁵Senckenberg Center for Human Evolution and Paleoenvironment, University of Tübingen, Tübingen, Germany

⁶Evolutionary Studies Institute, University of the Witwatersrand, Johannesburg, South Africa

Correspondence

Magnus M. Haaland, Department of Archaeology, History, Cultural Studies and Religion, University of Bergen, Øysteinsgate 1, PO Box 7805, N-5020 Bergen, Norway.
 Email: magnus.haaland@uib.no

Scientific editing by Sarah Sherwood

Funding information

Fundação Amazônia Paraense de Amparo à Pesquisa, Grant/Award Number: 2017/16451-2; Norges Forskningsråd, Grant/Award Number: 262618; Deutsche Forschungsgemeinschaft, Grant/Award Number: MI 1748/1-1; FP7 Ideas: European Research Council, Grant/Award Number: 249587

Abstract

A complete Middle Stone Age ochre piece was unintentionally collected and fully preserved within a micromorphological block sample intended to characterise a 74 ± 3 ka occupation horizon at Blombos Cave, South Africa. Previously recovered ochre pieces from the same stratigraphic context (Still Bay) have displayed intricate modification patterns with significant behavioural implications. Yet, in the case of the trapped ochre, a direct visual assessment of its surfaces was impossible due to its impregnated state. In this study, we demonstrate how we successfully reconstructed three-dimensionally and characterised the block-sampled ochre piece using high-resolution microcomputed tomography scanning coupled with a range of microanalytical techniques, including optical petrography, micro-Fourier transform infra-red spectroscopy, micro-X-ray fluorescence and micro-Raman spectroscopy. Through a morphometric analysis of the score marks present on the trapped ochre's reconstructed surface, we were able to assess the types of modifications and the nature of the actions that created them. Our results show that a block sample-based study of archaeological artefacts allows for a comprehensive assessment of their depositional and microcontextual setting, their external morphology and microtopography, as well as their internal texture and geochemical properties. We suggest that this type of context-sensitive, multiscale and multidisciplinary investigation may also prove beneficial in the study of conventionally recovered archaeological artefacts.

KEYWORDS

geoarchaeology, micro-CT, micro-FTIR, micromorphology, micro-Raman, micro-XRF, Middle Stone Age, ochre

1 | INTRODUCTION

During the last decade, archaeological micromorphology has been successfully applied to an increasing number of Middle Stone Age (MSA) sites in southern Africa (e.g., Goldberg et al., 2009; Haaland et al., 2017; Karkanas et al., 2015; Larbey et al., 2019; Marean et al., 2000; Miller et al., 2013, 2016). Due to excellent preservation conditions, sediment samples collected at many of these sites typically contain large amounts of occupation debris derived from past human activities. Occasionally, larger artefacts (>1 cm) are also incorporated into the samples. Most often, this occurs as a result of an intentional sampling strategy in which archaeological deposits filled with occupation debris (e.g., fragments of bone, stone and organic material) and campsite features (e.g., hearths, shell middens and bedding) are purposefully targeted for microstratigraphic analysis.

On rare occasions, however, complete artefacts may be unintentionally sampled. In our case, an intact object (ca. 60-mm long) was collected as a part of a micromorphological block sample (BBC-13-16) originally intended to characterise a 74 ± 3 ka occupation horizon within the MSA sequence at Blombos Cave (BBC), South Africa (Figures 1 and 2). After this block sample was impregnated and cut open with a rock saw, we observed that besides its calcareous and quartz-rich sediments, it also contained a bright red, iron-rich rock fragment (Figure 3a). The profile shape and striking red colour of the fragment were clearly visible in the cut block sample (Figure 3b), as well as in the final thin sections (Figure 3c).

Morphologically, the trapped ochre piece resembles previously reported modified ochre artefacts recovered from BBC (Figure S1). In the thin section, the profile of the trapped ochre shows a highly irregular surface topography (Figure 3d). Its stratigraphic and depositional setting links it to the *Still Bay* technocomplex, an MSA phase known in BBC for its particularly rich ochre assemblage, including two pieces engraved with cross-hatched designs (Figures S1 and S2) (Henshilwood et al., 2002).

On the basis of these initial observations, we found it likely that a modified MSA ochre piece had been inadvertently collected and incorporated inside the BBC-13-16 micromorphological block sample. However, any direct visual inspection of its overall morphology and surface topography was impossible due to its impregnated, block-sampled state. To solve this problem, we decided to scan the entire micromorphological block, including the ochre piece within it, using X-ray microcomputed tomography (micro-CT). A micro-CT scanner generates multiple X-rays of physical objects that can be reconstructed into cross-sections or virtual three-dimensional (3D) models in a non-destructive way. In micromorphology, it has previously been used to document and inspect the internal composition and structure of a wide range of materials, including oriented soil and sediment samples (Ngan-Tillard and Huisman, 2017; Villagran et al., 2019).

This study aims to showcase how archaeological artefacts, when trapped inside impregnated block samples, can be digitally reconstructed in 3D. Furthermore, the incidental collection of the trapped ochre piece also presents us with a unique analytical

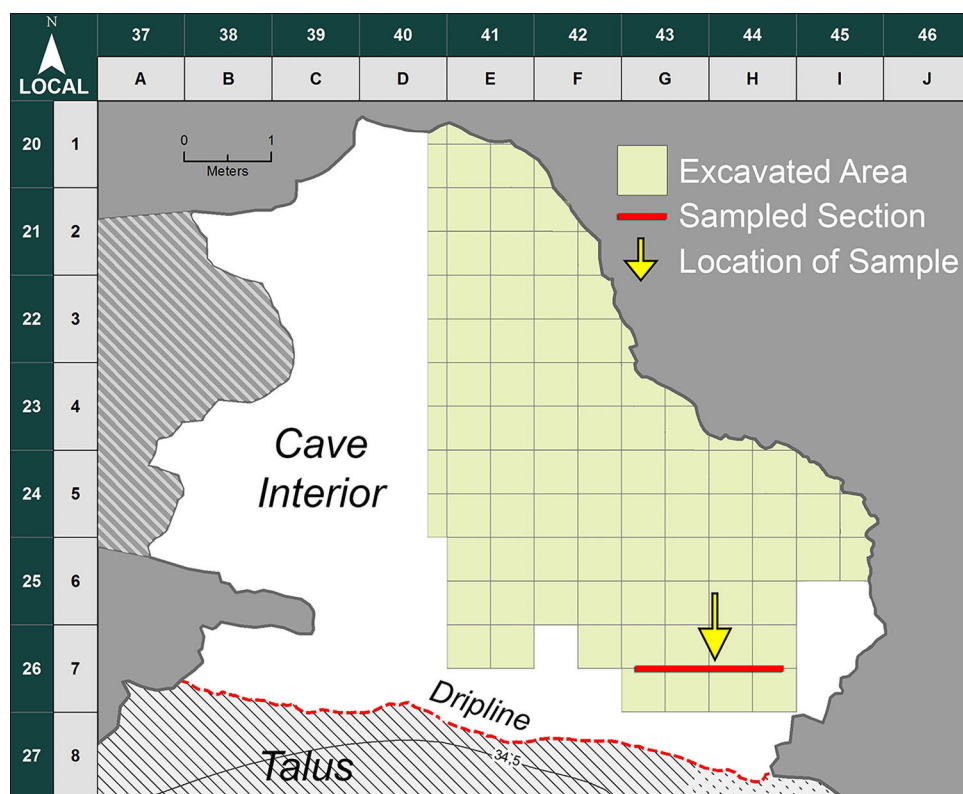


FIGURE 1 Site map of Blombos Cave. The red line shows the location of the sampled section wall (see Figure 2). Yellow arrow: Location of block sample that contained a red ochre fragment [Color figure can be viewed at wileyonlinelibrary.com]

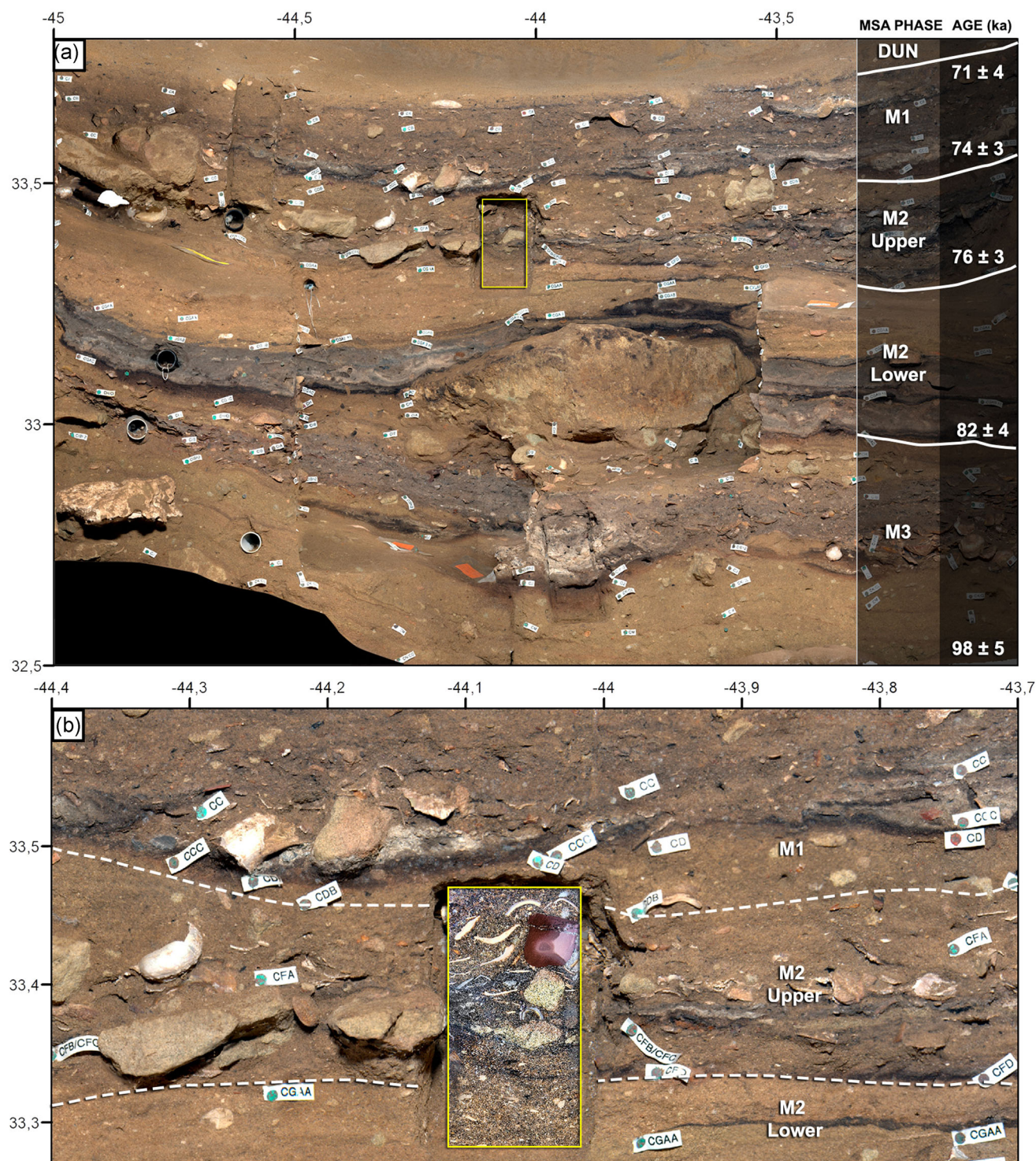


FIGURE 2 Southern section walls in Blombos Cave (BBC; see red line on Figure 1). (a) Overview of the Middle Stone Age sequence, occupation phases and dates. The yellow box indicates the location of the block sample (BBC-13-16). (b) A close-up view showing a georeferenced and scanned image of the cut open block sample containing a trapped ochre piece (red) [Color figure can be viewed at wileyonlinelibrary.com]

opportunity to study these important MSA artefacts from a range of new perspectives. For this reason, we use here a combination of archaeological micromorphology, 3D field photogrammetry and high-resolution micro-CT scanning, combined with a suite of micro-analytical techniques (micro-Fourier transform infrared spectroscopy

[FTIR], micro-X-ray fluorescence [XRF] and micro-Raman), to characterise the trapped ochre, both in terms of its depositional setting, its morphology, its microstructure and geochemical composition, as well as the nature and location of anthropogenic surface modifications.

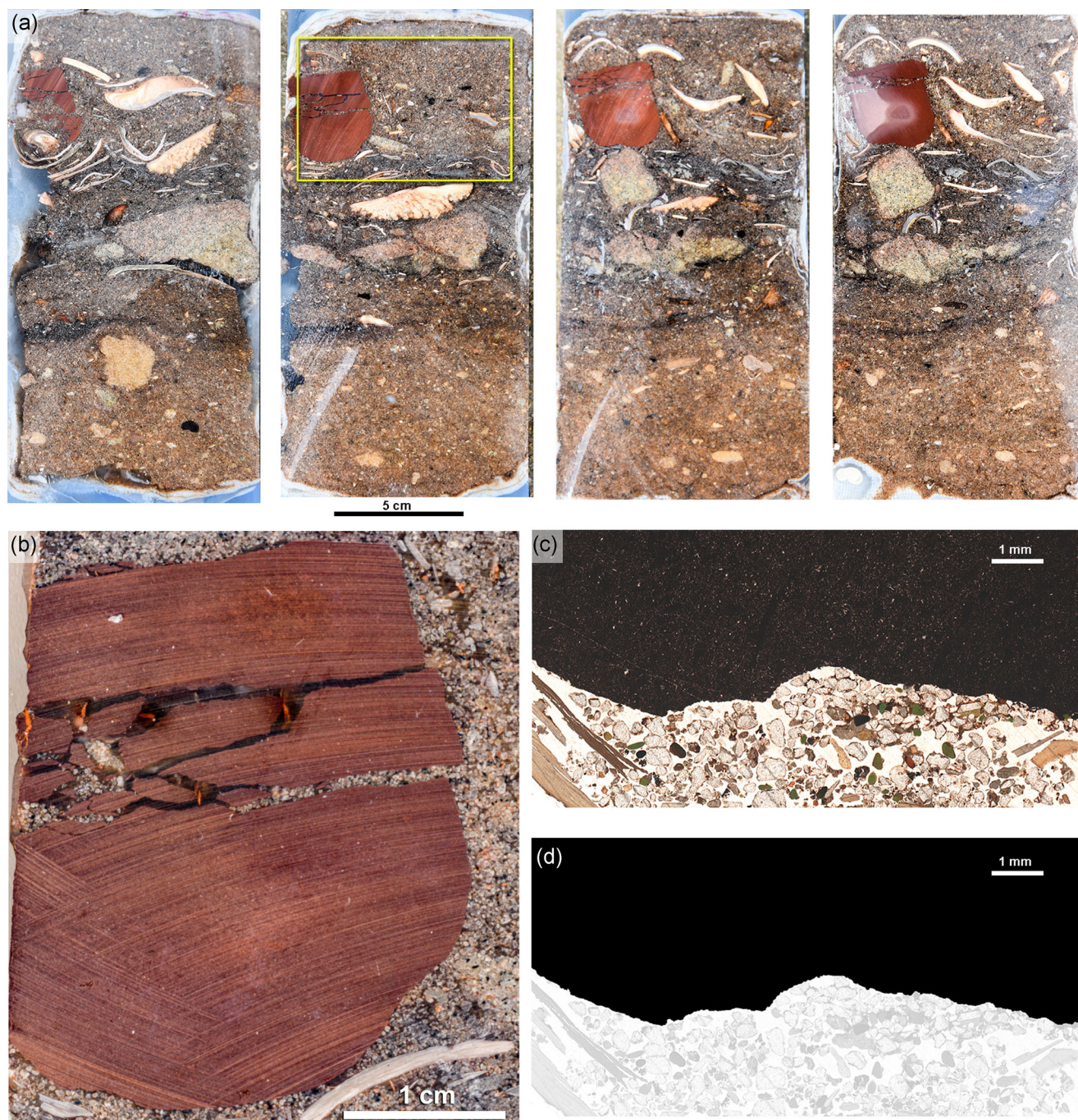


FIGURE 3 Documentation of the micromorphological block sample BBC-13-16. (a) Image scans of the four slabs that were cut from the original hardened block sample. The red ochre fragment is located at the top left corner. The yellow box indicates the part where a thin section chip was cut. (b) A close-up image section scan of the ochre piece is given in (a). The flattened and faceted surfaces of the ochre fragment can be observed. (c) A close-up view of the ochre piece and quartz-rich calcareous matrix surrounding in plane-polarised light. (d) The enhanced profile of the ochre in the thin section, showing a microtopography consistent with surface modifications [Color figure can be viewed at wileyonlinelibrary.com]

2 | BACKGROUND

2.1 | Ochre in Middle Stone Age contexts

Ochre is a colloquial term used to describe a series of ferruginous rocks that were intentionally collected and modified by humans from ca.

300 ka (Barham, 2002; Hovers et al., 2003; McBrearty & Tryon, 2006; Watts et al., 2016; Watts, 2010). These rocks, clays and sediments typically contain varying amounts of iron oxides (generally FeO, FeO₂ or Fe₂O₃) or oxide-hydroxides (α -FeOOH) that can produce yellow, orange, brown, red, purple and black-coloured streaks (Barham, 2002; Cornell & Schwertmann, 2003; Erlandson et al., 1999; Hodgskiss,

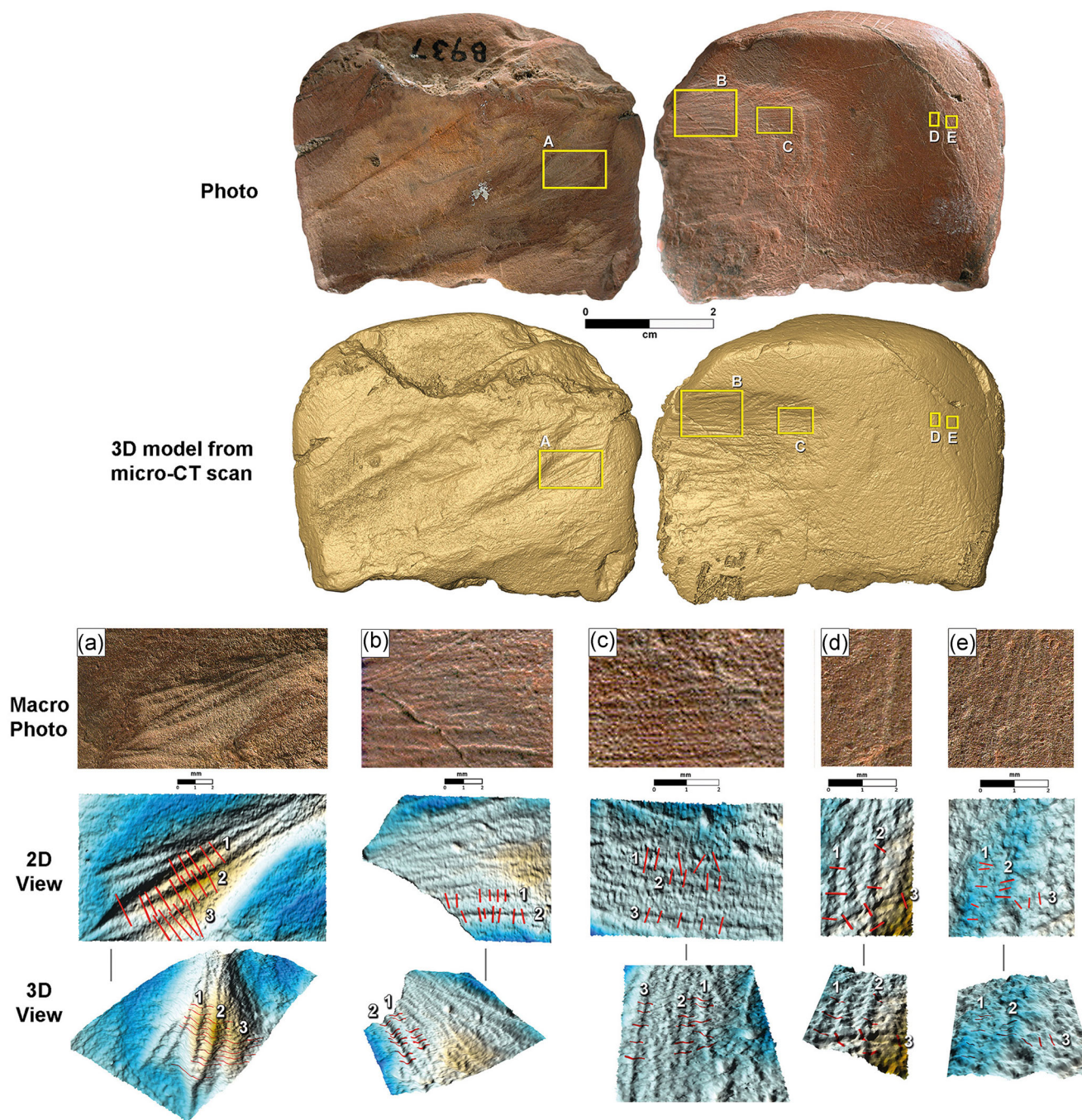


FIGURE 4 Top: Photos and three-dimensional (3D) models (yellow) showing the front and backside of the modified ochre piece SAM-AA 8937. Yellow rectangles indicating areas selected for close-up photos and corresponding 3D microtopographic models (seen in 2D and 3D view) of: (a) Deep and wide scoring, (b) scoring, (c) scoring (line 1) and striations (line 2 and 3), (d) striations and (e) microstriations. The location and direction of crosscuts and from where profile heights, lengths and angles were measured, are indicated with red lines. Multiple measurements were conducted along with the same scoring or striation (indicated by line numbers) [Color figure can be viewed at wileyonlinelibrary.com]

2013; Hovers et al., 2003; Watts, 2002, 2009). In southern Africa, its occurrence has been reported from ca. 160 ka (Marean et al., 2007) and from where its presence has then become ubiquitous at sites across this region (Watts, 1998, 2009; Wolf et al., 2018).

The antiquity and abundance of ochre at MSA sites have often been associated with the emergence of symbolic behaviours (d'Errico et al., 2003; Henshilwood, 2007; Watts, 2009). Yet, the precise

nature of symbolic pigment is difficult to assess from the current archaeological record, for example, as paint on human skin or artefacts. However, recent research on the operational chains of ochre collection and processing has provided insight into the behavioural and technological aspects behind pigment production. Studies of modified MSA ochres typically show striated surfaces from intensive grinding, which are widely assumed to represent evidence for

pigment (powder) extraction (Hodgskiss, 2010, 2012). In addition, both ethnographic accounts (Molefe, 2015; Rifkin, 2015b) and recent experimental works (Hodgskiss, 2010; Rifkin, 2012; Wadley, 2005) have resulted in more functional interpretations of ochre uses, for example, as an insect repellent (Rifkin, 2015a), sunscreen (Rifkin et al., 2015), as a hide-tanning agent (Rifkin, 2011) or as an ingredient in hafting mastics (Lombard, 2006, 2007; Wadley et al., 2004; Zipkin et al., 2014).

Ochre residues on a range of non-ochre MSA artefacts, such as lithics (Lombard, 2006, 2007; Wojcieszak & Wadley, 2018, 2019), stones (Henshilwood et al., 2018; Villa et al., 2015), shells (d'Errico et al., 2015; Henshilwood et al., 2004; Henshilwood, Sealy, et al., 2011; Vanhaeren et al., 2013), bones (Badenhorst et al., 2016; Henshilwood, d'Errico, et al., 2001; Henshilwood, Sealy, et al., 2001) and human teeth (Harvati et al., 2015), attest to the significance of ochre pigments and their multifaceted use during the African MSA.

2.2 | Blombos Cave and its Middle Stone Age ochre assemblage

Blombos Cave is located ca. 300 km east of Cape Town on the southern coast of South Africa. It contains more than 3 m of laminated deposits dated to ca. 101–70 ka (Henshilwood et al., 2011; Jacobs et al., 2020; Tribolo et al., 2006). The MSA sequence has been divided into four occupation phases, of which the upper two—M1 and M2 upper—are associated with the *Still Bay technocomplex* and dated to ca. 76–71 ka (Jacobs et al., 2020).

Around 8000 pieces of primarily red ochre are reported from the MSA levels, of which 1,500 are >10 mm in length (Henshilwood, Sealy, et al., 2001; Watts, 2009). The majority of the anthropogenically modified ochres ($n = 1534$) are deep, saturated shades of red (Watts, 2009). Although most of the ochres recovered from BBC are associated with the upper M3 occupation levels dated to ca. 84 ka, a considerable amount of modified ochre ($n = 254$) is also found in the M1 and M2 upper phases, that is, the *Still Bay* phase. Two modified ochre pieces from the M1 phase display cross-hatched scorings in combination with parallel incised lines (Henshilwood et al., 2002). Henshilwood et al. (2009) argue that the geometric arrangement of the score marks on these pieces represents engravings that may constitute a premeditated pattern or design, as both pieces appear to have been subjected to highly consistent scoring pressure, indicating that the lines were produced in a precise and controlled manner.

A range of other artefacts associated with ochre is also reported from BBC. Henshilwood et al. (2018) report a silcrete flake displaying a cross-hatched pattern drawn on with an *ochre crayon* from the *Still Bay* levels. Several ochre-stained and perforated marine shell beads are documented from the same levels (d'Errico et al., 2005, 2015; Henshilwood et al., 2004; Vanhaeren et al., 2013). Additionally, excavators have also recovered an in situ ochre toolkit consisting of ground ochre powder, seal bone and charcoal mixed into a liquid compound and kept inside two abalone shell containers from the lowermost level of the cave, dated to ca. 101 ka (Henshilwood et al., 2011).

3 | ANALYTICAL SCOPE

In this study, we characterise the trapped ochre fragment in the following contexts:

- (1) Archaeological field context—by visually and spatially contextualising the ochre within its original location in the cave and its associated occupational phase;
- (2) Archaeological microcontext—by analytically and spatially situating the ochre within the microlaminated occupation deposits that physically surround it;
- (3) Physical properties—by reconstructing its size, shape, texture, internal structure as well as its elemental and mineralogical composition;
- (4) Anthropogenic surface modifications—by documenting and analysing the occurrence, location and physical properties of scoring marks and striations.

For the interpretation of the trapped ochre fragment, two conventionally recovered and previously described ochre pieces (SAM 8937 and SAM 8938) were selected for morphometric comparison (Henshilwood et al., 2002, 2009). These two reference ochre pieces are from the same occupation phase as the trapped ochre (*Still Bay*) and were recovered only 1.3 m away from the ochre in the block sample (Figure S2). Both reference ochre pieces were ground and faceted before being scored (Henshilwood et al., 2002) and Henshilwood et al. (2009) also report—besides the occurrence of engravings—the presence of microstriations and striations on their surfaces.

4 | METHODS

4.1 | Archaeological field context (macroscopic)

The MSA occupation deposit (M2 upper) associated with the block sample containing the trapped ochre (BBC-13-16) was first excavated in 2011 and then again in 2019. We used field notes and photographs taken during these field seasons, in combination with image-based 3D modelling techniques (Unhammer, 2016), to reconstruct and characterise the sedimentary matrix and depositional setting in which the ochre piece was recovered.

4.2 | Micromorphology and archaeological microcontext

The block sample (BBC-13-16) was collected from the exposed southern section wall of BBC (Figure 2). It was stabilised by plaster bandage, before being transported to the University of Tübingen, Germany, where it was impregnated with resin under vacuum, in a 7:3 mixture ratio of unpromoted polyester resin (Viscovoss N 55S) and styrene, in addition to 5-ml/L hardener (methyl ethyl ketone peroxide). The hardened block sample was sliced into four slabs

(Figure 3a), one of which was selected for thin sectioning (60×90 mm, $30\text{-}\mu\text{m}$ thickness). It should be noted that during the slicing of the impregnated block sample, some of its original thickness, including the trapped ochre piece, was removed by the saw blade (>10 mm). By applying thin section-wide documentation procedures described by Haaland et al. (2019), and by following general (Courty et al., 1989; Stoops, 2003) and site-specific descriptive protocols (Haaland, 2018), we characterise the sedimentary composition and microstratigraphic configurations.

4.3 | Micro-CT scan and 3D surface reconstruction

Each of the block sample slabs (four in total) was individually scanned with micro-CT at the General Electric office in Stuttgart with a Phoenix v|tome|x m CT scanner (General Electric) at 250 kV, 220 mA and an isotropic resolution of 0.0397 mm. Segmentation of each micro-morphological slab ($n = 3$) was performed automatically using thresholds optimised for best segmentation results in Avizo 8.1 (Thermo Fisher Scientific—FEI). The removal of the pervasive nonochre material, such as attached quartz grains, finer calcareous sediments and resin, was done manually. A tri-dimensional surface (i.e., a cloud of 3D points connected by triangles) was obtained from each segmented volume by allowing for maximal and unconstrained smoothing (level 9 in the function “Surface Gen”). Finally, the ochre pieces that were inside the micromorphology block were combined and manually aligned to restore the overall morphology of the original piece before it was cut.

We also conducted high-resolution micro-CT scanning on the two reference ochres from BBC (SAM 8937 and SAM 8938) (Henshilwood et al., 2002, 2009). These scans took place at the Microfocus CT Laboratory (Evolutionary Studies Institute), the University of the Witwatersrand, South Africa. Scanning was performed with a Nikon XTH 225/320 LC with a Perkin Elmer flat panel detector at 90 kV, 220 mA and isotropic resolutions of 0.0346 and 0.0498 mm. From these scans, we created two digital 3D models that were generated and rendered in the same way as the trapped ochre piece, thus providing us with a comparative data set.

4.4 | Microanalytical techniques

Micro-XRF analyses were conducted on the thin section and corresponding slab, enabling the creation of elemental distribution maps using a Bruker M4 Tornado benchtop instrument.

Analyses occurred under full vacuum (20 mbar), with no filters, an Rh tube voltage of 50 kV and 600 mA current, and a detection range of $0\text{--}40$ keV. The average spot size is $20\text{ }\mu\text{m}$; pixel spacing and dwell time varied from 8 to $60\text{ }\mu\text{m}$ and 10 to 300 ms, respectively, depending on the mapping area. We used one of the two silicon drift detectors in the system that is optimised for quantitative analyses, calibrated the instrument using a zirconium standard and checked the instrument function using measurements on internal steel, glass and copper standards. The reported elements (see Table 1) were selected by manually

observing the presence or absence of K- and L-lines in the average spectrum generated over the entire mapping area and on the maximum pixel spectrum generated on maps of the ochre only.

The elements were subject to a modified version of the Bruker “oxides”—a quantification method that presents the results as wt% oxides. The formulae listed in parentheses in Table 1 after the elements indicate the oxides that were used in the wt% and norm. wt % calculations. Rh, which is present in the instrument itself, is used only in the deconvolution. In this study, we quantified the elemental composition of seven ochre fragments (originally belonging to a single ochre artefact) by conducting deconvolution on average spectra generated from an area corresponding to each of their surfaces (see outlines of measured fragments 1–7 in Figure S5). Quantitative results were generated from areas that met or exceeded 300 s of analytical time. The elemental mapping allowed a visual observation of the distribution of elements within the fragments, and additionally, transects were generated from the maps to evaluate minor fluctuations in element abundance along different planes.

For the mineralogical characterisation, we used FTIR on a few micrograms of ochre powder, obtained by scraping the internal edge of the ochre within the already cut chip. The instrument used was a Cary 660 bench FTIR spectrometer (Agilent Technologies). The measurements were conducted in both transmission mode and in attenuated total reflectance (ATR) mode (64 scans at 4 cm^{-1} resolution), allowing us to define absorption peaks in the frequency area of $4400\text{--}400\text{ cm}^{-1}$. For transmission mode measurements, the ochre sample was ground into a powder using an agate mortar and pestle. Approximately 0.1 mg of sample was mixed with 0.5 mg of KBr powder and then pressed into 7-mm pellets using a hand press. The FTIR spectra were processed and analysed using the Agilent Resolutions Pro software and compared with in-house references and other available reference libraries (Lafuente et al., 2016; Weiner, 2010). Spectra were also collected directly off the chip and petrographic thin section using the FTIR microscope (Cary 610) attached to the same instrument in reflectance mode and using a diamond crystal ATR accessory (Agilent Pike Gladi-ATR Vision). Raman spectra were obtained using a confocal Raman spectrometer (Horiba Jobin-Yvon Labram-HR) attached to a petrographic microscope and collected in the spectral range between 150 and 1500 cm^{-1} using 514-nm laser wavelength (25 s exposure time and 25 acquisitions). The measurements were collected through a $50\times$ objective on a confined area of the thin section containing the ochre ($c. 5\text{ }\mu\text{m}^2$).

4.5 | Digital reconstruction and quantitative characterisation of ochre surfaces

Although there are few high-resolution investigations of surface modifications on ochre (but see Rosso et al., 2017), a quantitative cut mark analysis has a long history within faunal taphonomy (Binford, 1981; Lartet & Christy, 1875; Shipman, 1981). Particularly relevant for this study is the development of morphometrical analysis of cutmarks using high-resolution 3D digital recording methods,

TABLE 1 Results of m-XRF analysis of the trapped ochre piece

| Element | Fragment 1 | | Fragment 2 | | Fragment 3 | | Fragment 4 | | Fragment 5 | | Fragment 6 | | Fragment 7 | | Average (n = 7) | |
|--------------------------------------|-------------|--------|------------|--------|------------|--------|------------|--------|------------|--------|------------|-------|------------|--------|-----------------|--------|
| | Net | wt% | Net | wt% | Net | wt% | Net | wt% | Net | wt% | Net | wt% | Net | wt% | Net | wt% |
| Al (Al ₂ O ₃) | 1,171,299 | 8.175 | 130,572 | 8.023 | 361,373 | 8.018 | 46,197 | 8.072 | 35,564 | 8.412 | 224,901 | 8.58 | 696,591 | 8.619 | 380,928 | 8.271 |
| As (As ₂ O ₃) | 32,017 | 0.003 | 4557 | 0.004 | 12,531 | 0.004 | 1162 | 0.003 | 1063 | 0.004 | 6754 | 0.00 | 17,391 | 0.003 | 10,782 | 0.004 |
| Ca (CaO) | 199,756 | 0.089 | 43,683 | 0.173 | 101,798 | 0.145 | 11,090 | 0.123 | 7414 | 0.115 | 33,094 | 0.08 | 93,826 | 0.075 | 70,094 | 0.115 |
| Cr (Cr ₂ O ₃) | 86,952 | 0.011 | 9569 | 0.011 | 27,294 | 0.011 | 3215 | 0.010 | 2087 | 0.009 | 16,323 | 0.01 | 49,658 | 0.012 | 27,871 | 0.011 |
| Cu (Cu ₂ O) | 25,992 | 0.003 | 2586 | 0.003 | 7212 | 0.003 | 666 | 0.002 | 49 | 0.000 | 3885 | 0.00 | 12,973 | 0.003 | 7623 | 0.002 |
| Fe (Fe ₂ O ₃) | 117,564,551 | 12.702 | 13,023,629 | 12.421 | 36,933,388 | 12.800 | 4,788,313 | 13.106 | 3,345,479 | 12.332 | 21,419,480 | 12.77 | 65,968,661 | 12.731 | 37,577,643 | 12.695 |
| Mg (MgO) | 5069 | 0.121 | 369 | 0.078 | 1162 | 0.088 | 44 | 0.026 | 31 | 0.025 | 317 | 0.04 | 1490 | 0.063 | 1212 | 0.063 |
| Mn (MnO) | 0 | 0.000 | 0 | 0.000 | 0 | 0.000 | 0 | 0.000 | 0 | 0.000 | 0 | 0.00 | 0 | 0.000 | 0 | 0.000 |
| O | 0 | 32.802 | 0 | 32.759 | 0 | 32.652 | 0 | 32.228 | 0 | 33.523 | 0 | 33.56 | 0 | 33.651 | 0 | 33.024 |
| P (P ₂ O ₅) | 0 | 0.000 | 0 | 0.000 | 0 | 0.000 | 0 | 0.000 | 0 | 0.000 | 0 | 0.00 | 0 | 0.000 | 0 | 0.000 |
| K (K ₂ O) | 2,867,204 | 2.227 | 315,546 | 2.175 | 880,770 | 2.179 | 112,278 | 2.167 | 84,378 | 2.271 | 529,433 | 2.28 | 1,654,764 | 2.312 | 920,625 | 2.230 |
| Rh | 407,426 | 0.000 | 47,304 | 0.000 | 129,852 | 0.000 | 16,662 | 0.000 | 12,215 | 0.000 | 78,892 | 0.00 | 234,364 | 0.000 | 132,388 | 0.000 |
| Si (SiO ₂) | 5,635,892 | 16.711 | 649,465 | 16.947 | 1,781,113 | 16.768 | 219,271 | 16.266 | 172,932 | 17.494 | 1,056,073 | 17.24 | 3,264,797 | 17.295 | 1,825,649 | 16.960 |
| Na (NaO) | 5495 | 0.617 | 452 | 0.449 | 722 | 0.259 | 132 | 0.372 | 13 | 0.050 | 0 | 0.00 | 263 | 0.053 | 1011 | 0.257 |
| Sr (SrO) | 60,337 | 0.007 | 8801 | 0.009 | 22,044 | 0.009 | 2667 | 0.008 | 1858 | 0.008 | 13,634 | 0.01 | 34,771 | 0.008 | 20,587 | 0.008 |
| S (SO ₃) | 0 | 0.000 | 0 | 0.000 | 560 | 0.002 | 0 | 0.000 | 0 | 0.000 | 0 | 0.00 | 0 | 0.000 | 80 | 0.000 |
| Ti (TiO ₂) | 1,532,335 | 0.350 | 179,487 | 0.364 | 507,463 | 0.370 | 60,948 | 0.347 | 48,114 | 0.380 | 298,899 | 0.38 | 849,533 | 0.348 | 496,683 | 0.362 |
| Zn (ZnO) | 62,942 | 0.007 | 6461 | 0.006 | 19,915 | 0.007 | 1998 | 0.006 | 1302 | 0.005 | 10,744 | 0.01 | 34,324 | 0.007 | 19,669 | 0.006 |
| Zr (Zr ₂ O ₂) | 67,358 | 0.009 | 7657 | 0.009 | 22,516 | 0.010 | 2762 | 0.010 | 1948 | 0.009 | 12908 | 0.01 | 37,945 | 0.009 | 21,871 | 0.009 |

Note: Seven individual fragments were measured, with outlines given in Figure 4b. The formulae listed in parentheses after the elements indicate the oxides that were used in the wt% and norm. Wt% calculations (see Tables S2–S8 for more detailed results).

Abbreviations: m-XRF, micro-X-ray fluorescence.

including the application of 3D digital microscopes (Bello & Galway-Witham, 2019; Bello & Soligo, 2008; Bello et al., 2011; Boschin & Crezzini, 2012; Braun et al., 2016; Wallduck & Bello, 2018), 3D laser scanning (Güth, 2012), micro-CT scanning (Bello et al., 2013) and microphotogrammetry (González et al., 2015). These 2D and 3D recording methods have proven to not only be accurate (Courtenay et al., 2018) but also applicable to a range of different types of surface modifications, other than butchering marks. Bello et al. (2013), for example, used a combination of digital 3D microscopy and micro-CT scanning to document and characterise intentional engravings on Magdalenian bone and antler, whereas Güth (2012) used 3D laser scanning to investigate Upper Palaeolithic incisions on slate plaquettes.

Here, we adopt a similar approach that allows us to physically measure and compare the modifications on the surfaces of the trapped ochre fragment with those found on the two reference ochre pieces. Specifically, we converted the 3D ochre models made from the micro-CT scans to digital elevation models (DEMs). We then imported these DEMs into mapping software (Surfer 16) and made them into digital microtopographic surfaces, allowing us to conduct metric measurements and to create profile crosscuts (i.e., red lines in Figures 4–6). We georeferenced the profile crosscuts using ImageJ and measured the height, width and angle of the profile shapes using a protocol (Figure 7) modified following Bello et al. (2013):

- Width of incision at the surface (W1): The maximal length between the two points where the inwardly sloping walls start to converge.
- Height of the incision (H1): The perpendicular depth of the incision relative to an imaginary, unaffected surface of the ochre.
- Width of the incision at one-third of the height (W2): The maximal length between two profile walls at one-third height of the full perpendicular depth.
- Angle of the impact (A): The angle between each inwardly sloping wall and the unaffected ochre surface.

The types of modifications we measured on the reference samples had already been qualitatively classified and reported by Henshilwood et al. (2009) on the basis of an assessment of their size, length, orientation, location and (co)occurrence. In this paper, we adopted their terminology and classification scheme, thus allowing us to define and compare ochre modifications on the reference pieces with those present on the trapped ochre piece in an analytically consistent way. The following categories were used: (I) microstriations, (II) striations, (III) scorings, (IV) deep scorings and (V) wide scorings. Additionally, we documented the morphometric properties of two types of engravings (Henshilwood et al., 2002): A thinner, shallower type (SAM 8937; Figure 5) and a thicker, deeper type (SAM 8938; Figure 6). It should here be noted that we do not think that our categories are representative of all types of ochre surface modifications found in the MSA ochre assemblage, as several archaeological and experimental ochre studies have previously demonstrated (Bernatchez, 2012; Henshilwood et al., 2009; Hodgskiss, 2010, 2013; Rosso et al., 2016).

5 | RESULTS

5.1 | Archaeological field context

The BBC-13-16 block sample contains deposits that cover three locally defined MSA occupation phases and five archaeostratigraphic units: CDB (M1 phase), CFA, CFB–CFC and CFD (M2 upper phase) and CGAA (M2 lower phase) (Figure 2). The trapped ochre fragment is associated with the M2 upper phase, being situated in the gradual transition between CFA and CFA–CFB (Figures 8 and 9). In the field, the M2 phase is defined by laterally extensive, laminated sandy deposits containing multiple combustion features and dark, organic-rich lenses associated with human occupation of the cave (Figure 2). Attesting to the intensity of occupation, extensive accumulation of shellfish, bone fragments (fish, tortoise, larger ungulates), ostrich eggshell and lithic artefacts (quartz and quartzite flakes dominate) can be seen in the section wall (Figure 2b) as well as on the exposed occupation surface (Figure 8b). In 2019, excavators recovered an approximately 8-cm long, modified ochre piece on the same occupation surface as the trapped ochre piece, some 20-cm away (Figure 8c,d).

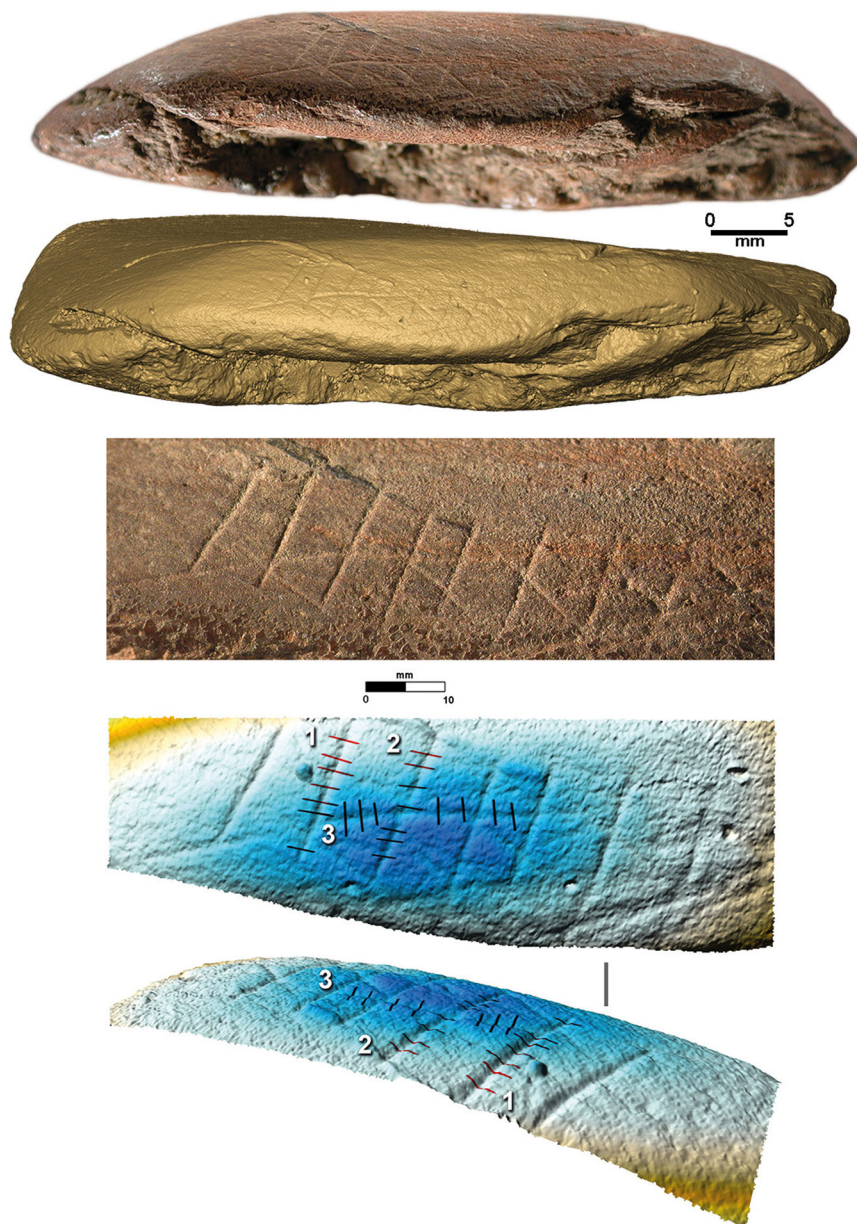
5.2 | Archaeological microcontext

The upper M2 microstratigraphy is characterised by a complex sequence of unconsolidated sandy deposits dominated by silt to sand-sized grains of sub-rounded quartz, glauconite grains and bioclastic material randomly dispersed within a microaggregated calcareous matrix (Figures 9 and 10). The sediments in which the trapped ochre is directly embedded are rich in anthropogenic coarse fraction (shellfish, burnt and unburnt bone, ochre fragments and charred material) and fine fraction, such as charred organic matter and wood-derived ash. The heat distribution model (Figure 10b) is generated on the basis of the distribution of unburnt (green) and burnt (red and black) glauconite grains, following the approach by Haaland et al. (2017). The interpolated heat map for the M2 upper phase shows that burnt sediments are frequently mixed with unburnt sediments throughout the sequence. Concentrated areas of burnt deposits are found in spatial association with the ash-rich features and with the deposits with higher concentration of human occupation debris.

5.3 | 3D reconstruction of the trapped ochre piece

A 3D reconstruction of the trapped ochre piece is shown in Figure 11. This composite model consists of three aligned submodels (I, II and III) and corresponds to each of the individually micro-CT-scanned slabs (Figure 3). The small gap between submodels represents the 2–3-mm cut of the rock saw blade. For individual submodel views of each ochre fragment (I, II and III), see Figure S3, and to view examples of unprocessed micro-CT images, showing crosscuts and the internal structure of the trapped ochre, see Figure S4. The ochre piece is broken into several fragments, with a slight gap

FIGURE 5 Top: Photo and three-dimensional (3D) model (yellow) showing the side view of the modified and lightly engraved ochre piece SAM-AA 8937. Middle: A close-up photo of a thin and shallow cross-hatched scoring (engraving). Bottom: 3D microtopographic models (seen in 2D and 3D view) showing the location and directions of profile crosscuts along three different lines [Color figure can be viewed at wileyonlinelibrary.com]



between their surfaces. We estimate the minimum original size of the ochre piece to be ca. $5.9 \times 3.2 \times 3.7$ cm (see Table 2 and Figure S1). The elongated morphology of the trapped ochre is broadly rectangular, having three flat sides (Sides A and C and the bottom part), whereas the top part displays a convex profile shape. This morphology appears to be uniform throughout the different sections of the piece (Figures S3 and S4).

5.4 | Microanalytical characterisation of the trapped ochre piece

5.4.1 | Texture and colour

The ochre surface, as observed in the block sample, exhibits a dusky red colour (Munsell 5R 3/4). In the thin section (reflected light), the

trapped ochre displays a rusty brown colour, whereas, in plane-polarised light, it appears opaque (Figure 12). In cross-polarised light, especially under high magnification, the matrix takes on a deeper, reddish-brown character. The dark and massive microstructure contains colourless silt-sized and microcrystalline quartz that displays undulatory extinction and low interference colours under cross-polarised light.

5.5 | Elemental and mineralogical characterisation

Micro-XRF elemental distribution maps were produced from the petrographic thin section (Figure 13a). These maps showed the relative abundance of elements in the ochre piece, relative to the surrounding sedimentary matrix, and within the piece itself. Compared with the sedimentary matrix which is rich in Ca, Si and P, the

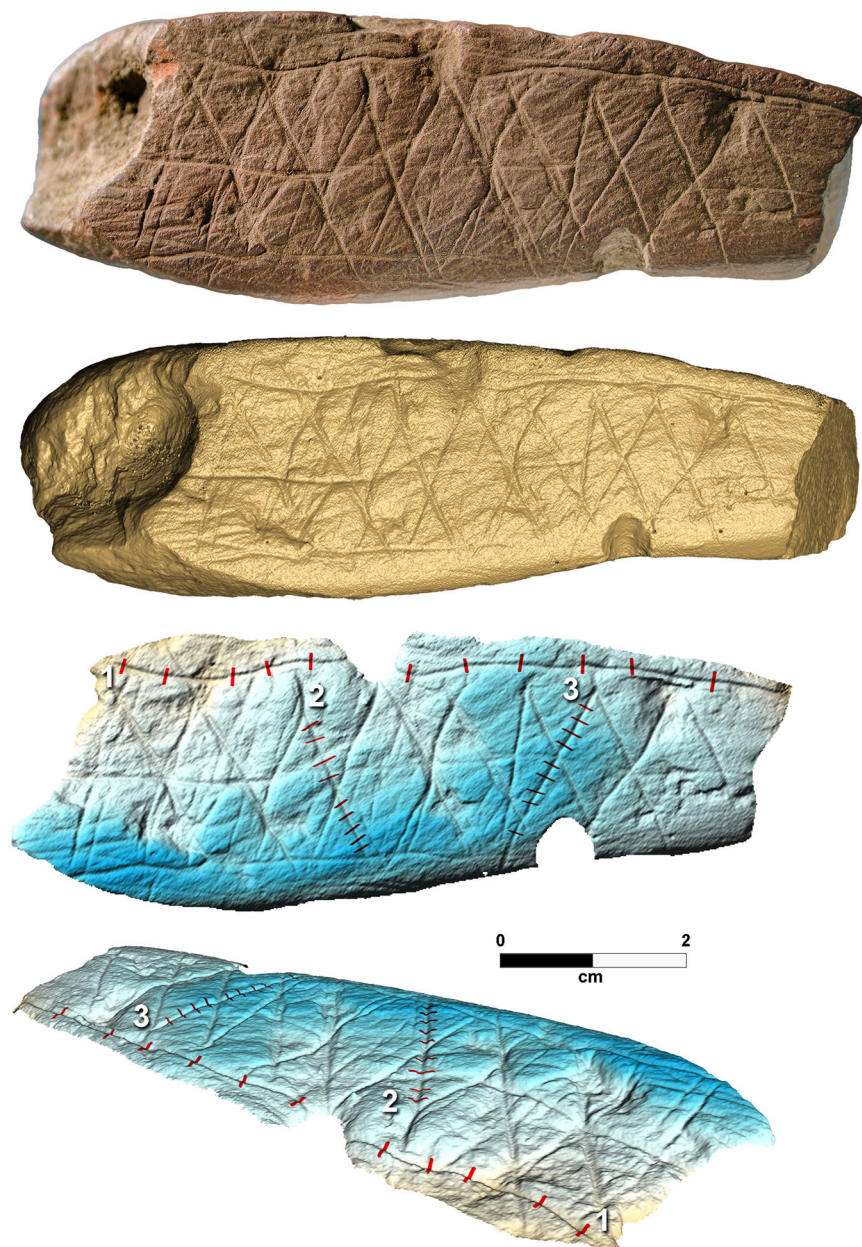


FIGURE 6 Top: Photo and three-dimensional (3D) model (yellow) showing the side view of the modified and engraved ochre piece SAM-AA 8938. Bottom: 3D microtopographic models (seen in 2D and 3D view) showing the location and directions of profile crosscuts (red lines) along three different scoring lines [Color figure can be viewed at wileyonlinelibrary.com]

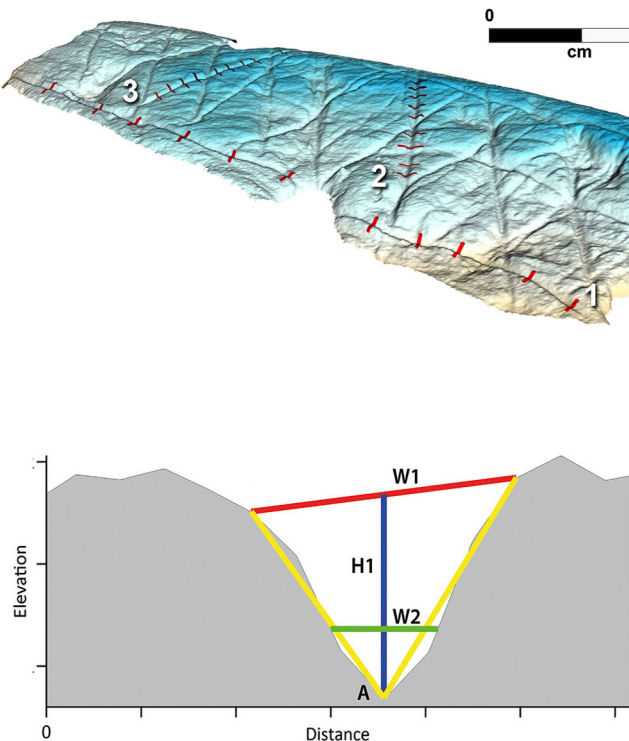


FIGURE 7 Protocol for measuring the height, width and angle of ochre surface modification marks using high-resolution profile views. A, angle of mark; H1, maximum height; W1, maximum width; W2, width at one-third of maximum height [Color figure can be viewed at wileyonlinelibrary.com]

trapped ochre piece shows high concentrations of Al (11%), Fe (10%), K (3.3%), Si (27%) and Ti (0.5%) (Figure 13b,c and Tables 1, S2–S8). Manganese (Mn) is absent in the ochre. The different ochre fragments ($n = 7$) all have the same elemental composition with only minor fluctuations (Table 1 and Figure S5).

Transects were drawn to investigate spatial trends in the abundance of elements moving from the centre of the piece towards the exterior in several directions and from the centre or edges of the piece towards planes of weakness (cracks) (Figure S6). There were no enrichments or depletions in elements close to the outer surface of the piece or moving from the centre towards the planes of weakness (Figure S6). These results indicate that there is no diagenesis of the surface of this ochre piece after burial or compositional differences that could have contributed to fracturing. One of the transects revealed the presence of slight, but regular, fluctuations in relative

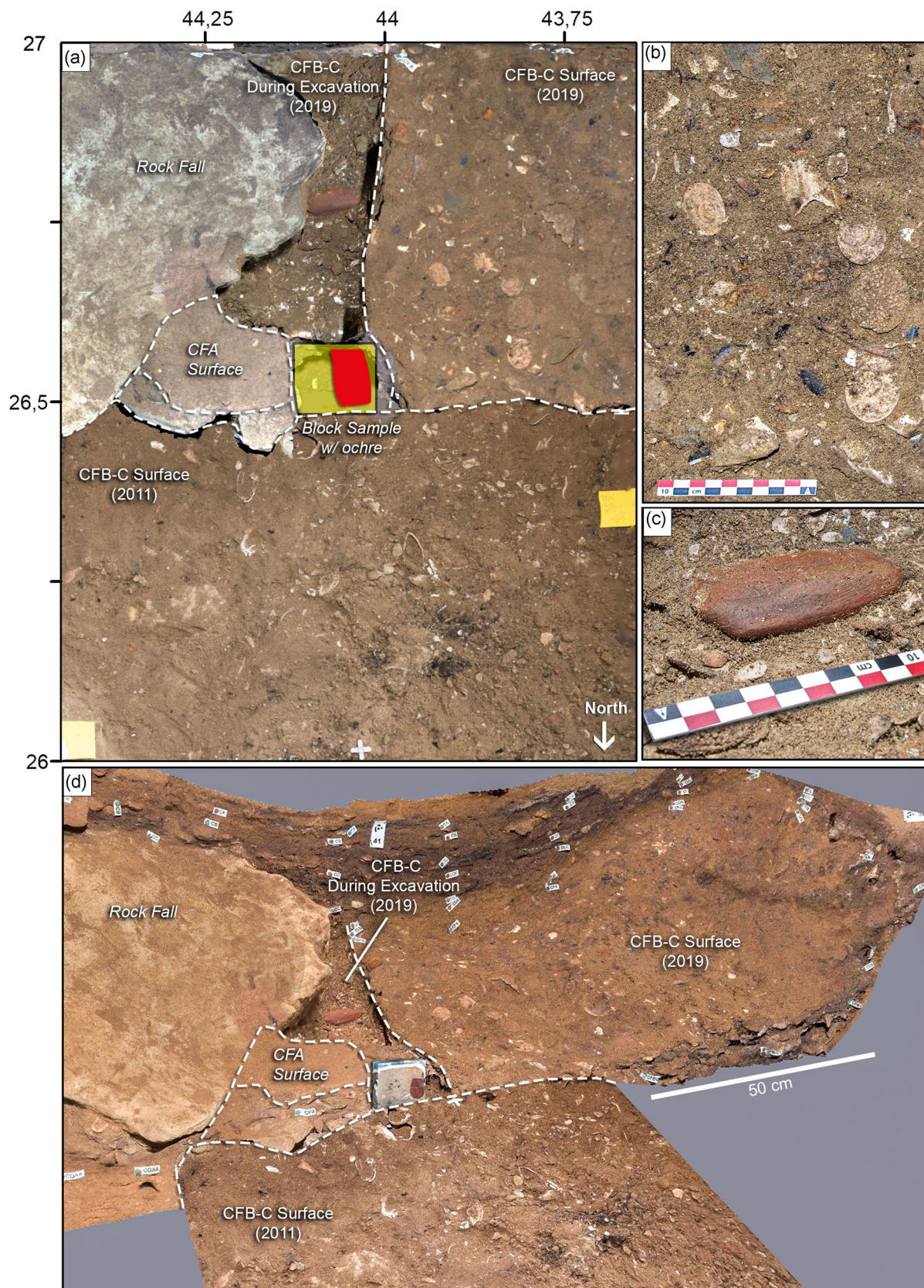


FIGURE 8 (Continued)

element abundance of titanium (Ti) and aluminium (Al). We suggest that the enrichment of Ti paired with depletion of Al may be indicative of internal laminations roughly 2.5 mm or less in thickness (Figure S7).

The FTIR spectra (Figure 14) show peaks corresponding to haematite (Fe_2O_3) at 536 and 459 cm^{-1} , which likely accounts for ca. 10% Fe content measured with the m-XRF. However, the shape of haematite peaks appears to be distorted due to the presence of kaolinite (540 and 471 cm^{-1}) and quartz (453 cm^{-1}). Besides these overlapping lower frequency peaks, we identified quartz based on the presence of peaks at 694 , 777 , 795 , 1056 , 1076 and 1163 cm^{-1} . Similarly, kaolinite was identified by the presence of the mid-range peaks at 695 , 775 , 916 , 1010 , 1034 and 1104 cm^{-1} , and three high-frequency absorption bands at 3695 , 3655 and 3612 cm^{-1} , all of which are associated with the stretching vibrations of hydroxyl groups. The micro-Raman spectrum (Figure 15) illustrates the presence of haematite more clearly. Within the 150 – 1500 cm^{-1} spectral domain, we see the following peaks: 216 , 288 , 400 , 601 and 1320 cm^{-1} , all which can be assigned to haematite ($\alpha\text{-Fe}_2\text{O}_3$) (Buzgar et al., 2009, 2013; Lafuente et al., 2016).

5.6 | Microtopographic profile classification of surface modifications on ochre

Following the protocol in Figure 7, we conducted and measured 95 crosscuts (Figures 4–6) that provide profile views of microstriations, striations and scoring ($n = 64$) as well as engravings ($n = 49$) (Table 1). Representative profile shapes of each modification type are provided in Figure 16a–g. A boxplot showing the numerical spread and variation within and between each measurement category (angle, height and width) by the modification type is shown in Figure 16h (see Table 3 for summary statistics and Table S1 for raw data). It should be noted that the y-axis (i.e., the height of the profile) in Figure 16a–g has been amplified by an elevation factor of three ($z = 3\times$) to make the profile shapes more distinguishable. Although this uniform data set adjustment ensures that our comparative analyses are internally consistent, the values presented in Table 3 do not represent absolute, real-world values.

The profile shapes and boxplots in Figure 16 allow for visual and quantitative characterisation of the relative differences between each modification category. *Microstriations* represent small and shallow surface modifications that are $<0.1\text{ mm}$ in width (Table 3). This, along with their broad-angle measurements ($\bar{X} = 141.6^\circ$), makes them distinct from any of the other modification types. *Striations* are

larger than microstriations but are also small in size. Due to their relatively large height-to-width ratio, their angles are narrower ($\bar{X} = 101.4^\circ$) than those observed in microstriations. The profile shapes of *scorings* are similar to those of *striations* in terms of width, yet because they are considerably deeper, their angles are also narrower ($\bar{X} = 79.4^\circ$). Both *deep scorings* and *wide scorings* have notably larger height and width measurements than any other modification types. Their large dimension is also evident from their profile shapes, which often show shallow shoulders on each of the sidewalls (Figure 16f,g). Such shoulders may be indicative of repeated and multiple scoring movements. Although *deep scoring* marks have angles comparable to that of standard scorings, ($\bar{X} = 81.8^\circ$), their angles ($\bar{X} = 98.2^\circ$) are more comparable to *striations* and their width at one-third height (W2) is substantially greater than any other modification type. Morphometrically, the shallow cross-hatched engraving (SAM 8937) falls in between the categories of *striations* and *scoring*, whereas the deeper cross-hatching (SAM 8938) falls in between *scoring* and *deep scoring*.

To further compare the main modification types and the two engravings, we used multivariate statistics. Figure 17a shows a principal component analysis (PCA) of profile shape measurements ($n = 64$) by the type of modification. The first two principal components confirm that the three main modification types and the two sub-types generally form consistent and distinct shape-based groups. We also compared the profile shape measurements of the two cross-hatched engravings with the multivariate mean of the predefined modification types using a canonical discriminant function analysis (CDA) (Figure 17b). Qualitatively, the engravings of SAM8937 were defined as shallow (Henshilwood et al., 2009), and indeed, their profile shape measurements plot partially between the scoring and the striation categories and partially outside them (blue crosses in Figure 17b). Some of the shallow engraving measurements fall outside any of the categories, having slightly larger W1 and W2 values than the striations, and slightly wider angle than scoring. The engravings of SAM8938 were reported to be deeper and most likely made from repetitive and controlled hand motions. Again, the multivariate plots of their profile shape measurements support this qualitative assessment, as they regularly plot between the scoring and the deep scoring category (red circles in Figure 17b).

From these results, we conclude that our reference data set enables us to characterise and classify surface modifications as accurately and consistently as conventional qualitative assessments. Ultimately, this result enables us to apply our quantitative classification scheme on surface modifications we cannot physically observe, such as those present on the digitally rendered surface of the trapped ochre piece.

FIGURE 8 Macroscopic field context for block sample BBC-13-16. (a) A planar view of the occupation surfaces associated with the ochre fragment (red shape) inside the block sample (yellow rectangle). An approximately 7-cm long, red and highly modified ochre piece recovered during the 2019 field season and located c. 20-cm south of the original block sample location can be observed. (b) A close-up view of the 2019 ochre piece associated with the trapped ochre fragment. (c) A close-up view of the CFB-CFC occupation surface (note the scatters of shellfish [Sf], bone and lithic material). (d) A three-dimensional view and reconstruction of the occupation surfaces (CFA-CFB-CFC) associated with trapped ochre [Color figure can be viewed at wileyonlinelibrary.com]

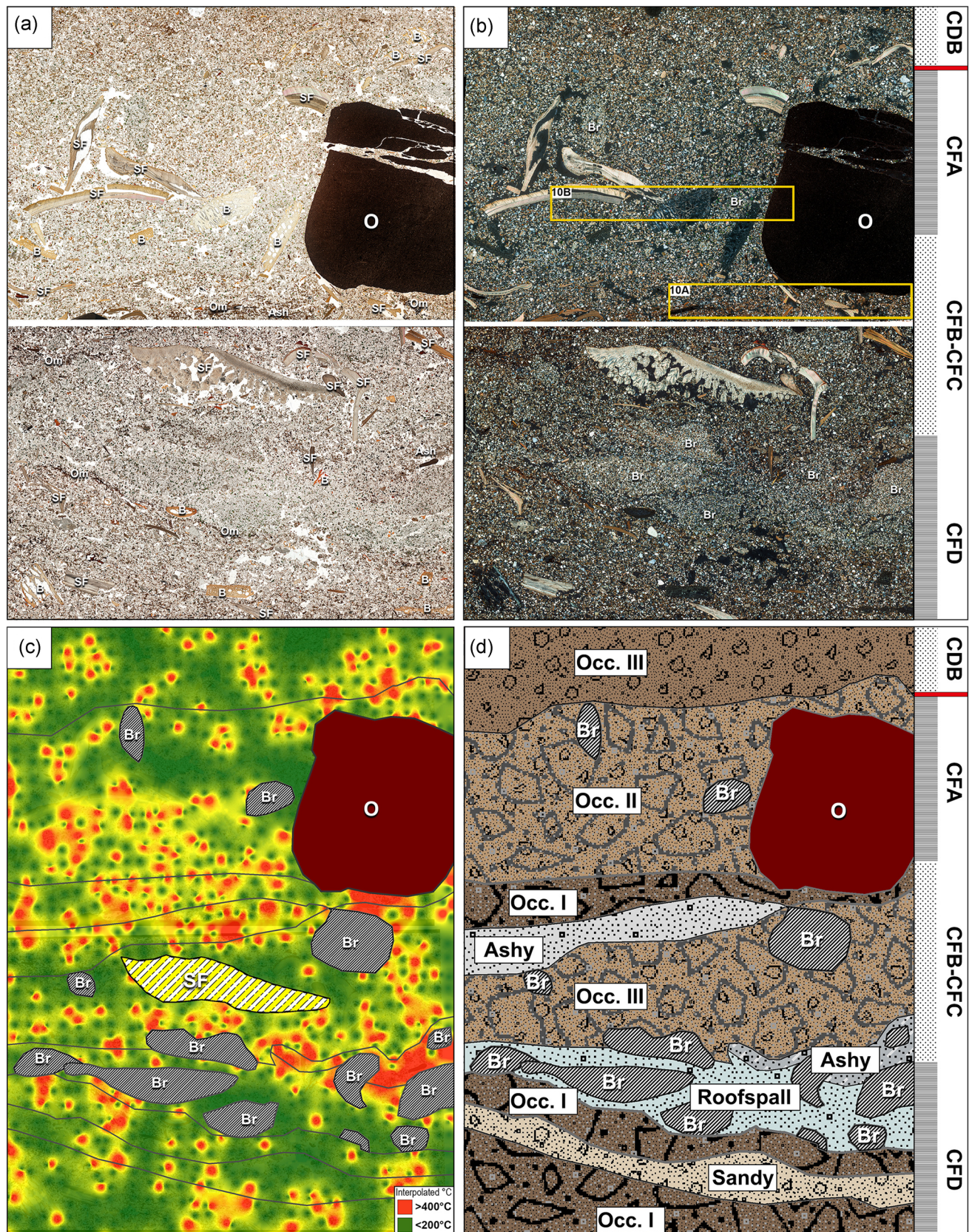


FIGURE 9 (Continued)

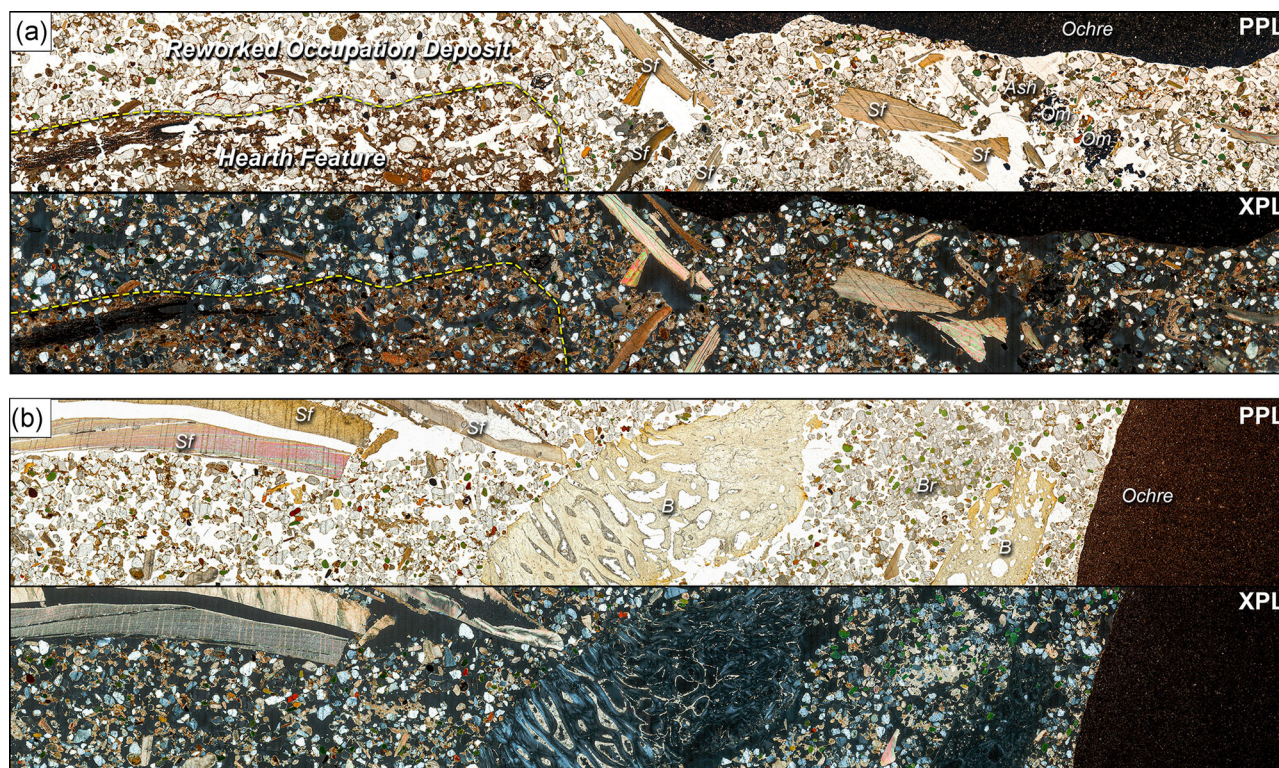


FIGURE 10 (a) A close-up view plane-polarised light/cross-polarised light (PPL/XPL) of the trapped ochre and the substrate on which it rests (see yellow outlines on Figure 9b). It should be noted that the reworked occupation deposit separates the ochre from the intact ash feature. Width = 4.5 cm. (b) The high-resolution thin-section scan (PPL/XPL) of the trapped ochre and sedimentary matrix in which it is embedded (note the mix of green (unburnt) and red (burnt) glauconite grains and the bone fragments lying angular positions). The width of the thin-section view = 4.5 cm [Color figure can be viewed at wileyonlinelibrary.com]

5.7 | Characterising surface modifications on the trapped ochre piece

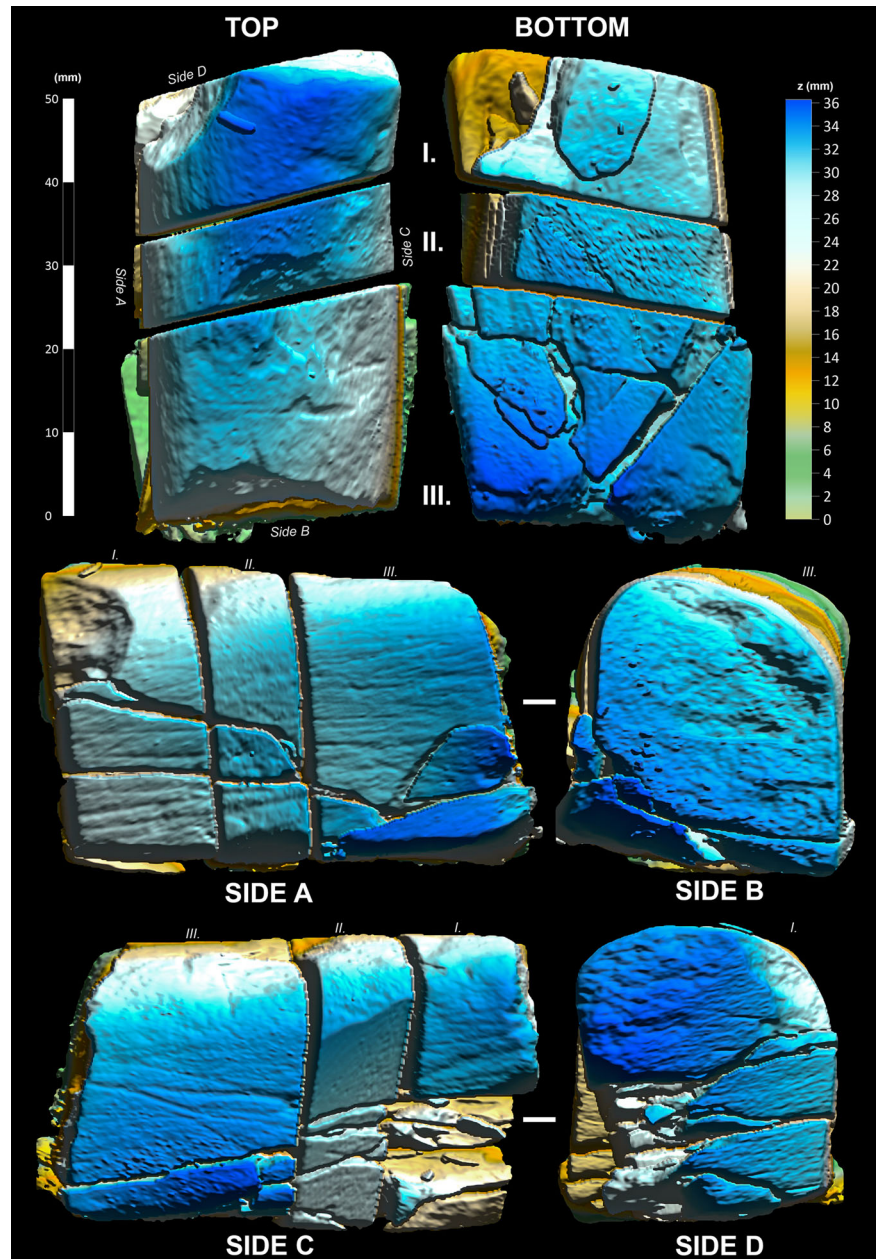
Figure 18a shows a low-resolution 3D reconstruction of Side C of the trapped ochre piece. Given its highly fragmented and shattered state, we re-rendered a smaller and more intact part of this model in a higher resolution. This high-resolution microtopographic model shows multiple surface modification marks of different sizes, of which we selected nine for profile shape measurements (red lines in Figure 18b,c). These nine measurements were then compared with the multivariate mean of the reference modification marks in a CDA (Figure 18d). From this comparison, we made the following classifications: Lines 1–2 and 6–9 fall into the *deep scoring* category, line 3 into *scorings*, line 4 into *wide scorings* and line 5 into *striations*. A visual reconstruction, showing our final classification of modification types

present on Side C of the trapped ochre, is provided in Figure 18e. For qualitative comparison, we also provide a close-up photo of a conventional MSA ochre piece displaying surface modifications comparable in size and orientation to those seen in Figure 18f.

Figure 19a shows a low-resolution 3D reconstruction of side A of the trapped ochre. This side was also heavily fragmented and shattered. We selected four areas with good surface preservation and 18 individual modification marks (i.e., lines) for a high-resolution profile shape analysis (Figure 19b–e). The profile measurements conducted on side A were compared to the reference modifications using two canonical plots (lines 1–9: Figure 19f; lines 10–18: Figure 19g). The results of our multivariate classification are provided in Figure 20a, which shows location and configuration of inferred modification types present on side A. Though several areas of Side A are covered with more striation marks than we selected

FIGURE 9 (a,b) The thin-section scan plane-polarised light and cross-polarised light of BBC-13-16 block sample showing anthropogenic material deposited in a quartz-rich calcareous matrix enriched with silt-sized organic material. Yellow outlines indicate close-up views in Figure 10a,b. B, bone; O, ochre; Om, organic matter; Sf, shellfish. (c) The heat map based on the distribution of burnt and unburnt glauconite. (d) Microcontextual analysis of block sample BBC-13-16 aligned with the macroscopic, archaeostratigraphic layers. M1: CDB, M2 Upper: CFA–CFD, M2 Lower: CGAA. Ashy, ash-rich deposits; Br, bedrock fragments; O, ochre; Occ., deposits enriched with human occupation debris to a high (I), medium (II) and low (III) degree. The width of the thin-section view = 8.2 cm. Archaeostratigraphic excavation units (e.g., CDB) indicated in the right margin [Color figure can be viewed at wileyonlinelibrary.com]

FIGURE 11 A combined three-dimensional (3D) reconstruction of the trapped ochre fragment inside block sample BBC-13-16. Each fragment (I, II and III) and each side (A, B, C, D, top and bottom) have been marked for later reference (see Figure S3 for 3D renderings of each individual fragment) [Color figure can be viewed at wileyonlinelibrary.com]



(e.g., piece III), we chose to target and reconstruct the deeper and more continuous modification marks, in particular those that are parallelly aligned to each other (Figure 20b). In Figure 20c, we present a tentative reconstruction of the trapped ochre piece and its deeper scoring marks, whereas, in Figures 20d and 20e, we provide

photos of an MSA ochre piece showing comparable modifications in terms of size and orientation.

Finally, we evaluated the spatial accuracy of 3D reconstructed ochre surface modifications by comparing their location and orientation with high-resolution edge profiles inferred directly from

TABLE 2 Dimensions (mm) and provenance of the trapped ochre fragment (BBC-13-16-O1) compared with two previously reported modified ochre pieces (Henshilwood et al., 2002) of comparable size and from the same occupation phase (Still Bay)

| ID | Recovery | Phase | Square | Layer | Length (mm) | Width (mm) | Thickness (mm) |
|--------------|-------------------|----------|--------|---------|-------------------|------------|----------------|
| BBC-13-16-O1 | Block sample | M2 Upper | H7a | CFB-CFC | 61.5 ^a | 31.8 | 36.5 |
| SAM-AA 8937 | During excavation | M1 | E6a | CC | 53.6 | 42.6 | 11.7 |
| SAM-AA 8938 | During excavation | M1 | H6a | CD | 75.8 | 34.8 | 24.7 |

^aWe estimate the length to be between 59 and 64 mm, depending on the cutting width of the rock saw blade (which can vary).

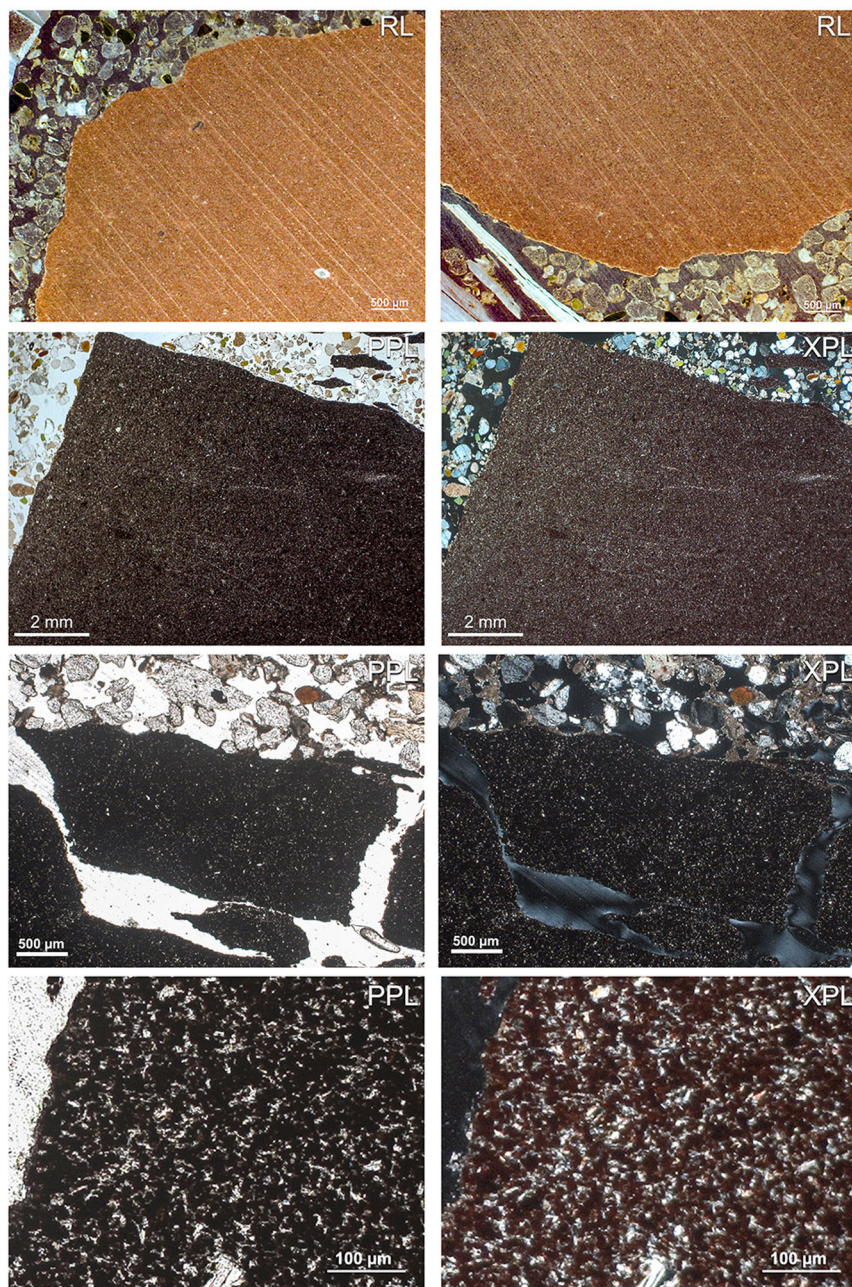


FIGURE 12 Thin section photomicrographs of trapped ochre (BBC-13-16-O1) in reflected light (RL), plane-polarised light (PPL) and cross-polarised light (XPL) at various magnifications. XRF, X-ray fluorescence [Color figure can be viewed at wileyonlinelibrary.com]

the physically trapped ochre (Figure 8a–c). Three parallel score marks were specifically selected for this procedure (lines 4–6 in Figure 19c). The results show that the score marks identified on the digitally rendered ochre piece align well with microtopographic profiles made from the physical ochre profiles (Figure 8d).

6 | DISCUSSION

6.1 | Archaeological and depositional setting

The BBC-13-16 block sample was collected ca. 1 m behind the cave drip line, in a part of the cave that functioned as a central activity area throughout all MSA occupation phases (Haaland, 2018). This

was also the case during the phase in which the trapped ochre was deposited, that is, the Still Bay phase. In general, the Still Bay is archaeologically associated with the earliest, but infrequent, occurrences of bifacially worked stone points (Villa et al., 2009), polished bone points (Henshilwood et al., 2001; d'Errico & Henshilwood, 2007), perforated marine shell beads (d'Errico et al., 2005; Henshilwood et al., 2004; Vanhaeren et al., 2013) and at least two engraved ochre pieces (Henshilwood et al., 2009); however, numerous other modified and nonmodified ochre artefacts are also reported (Henshilwood, Sealy, et al., 2001; Henshilwood et al., 2002; Watts, 2009).

The archaeostratigraphic unit (CFB–CFC) directly below the trapped ochre piece contains multiple elongated hearth features and shell-rich deposits. These features are clearly visible in the section

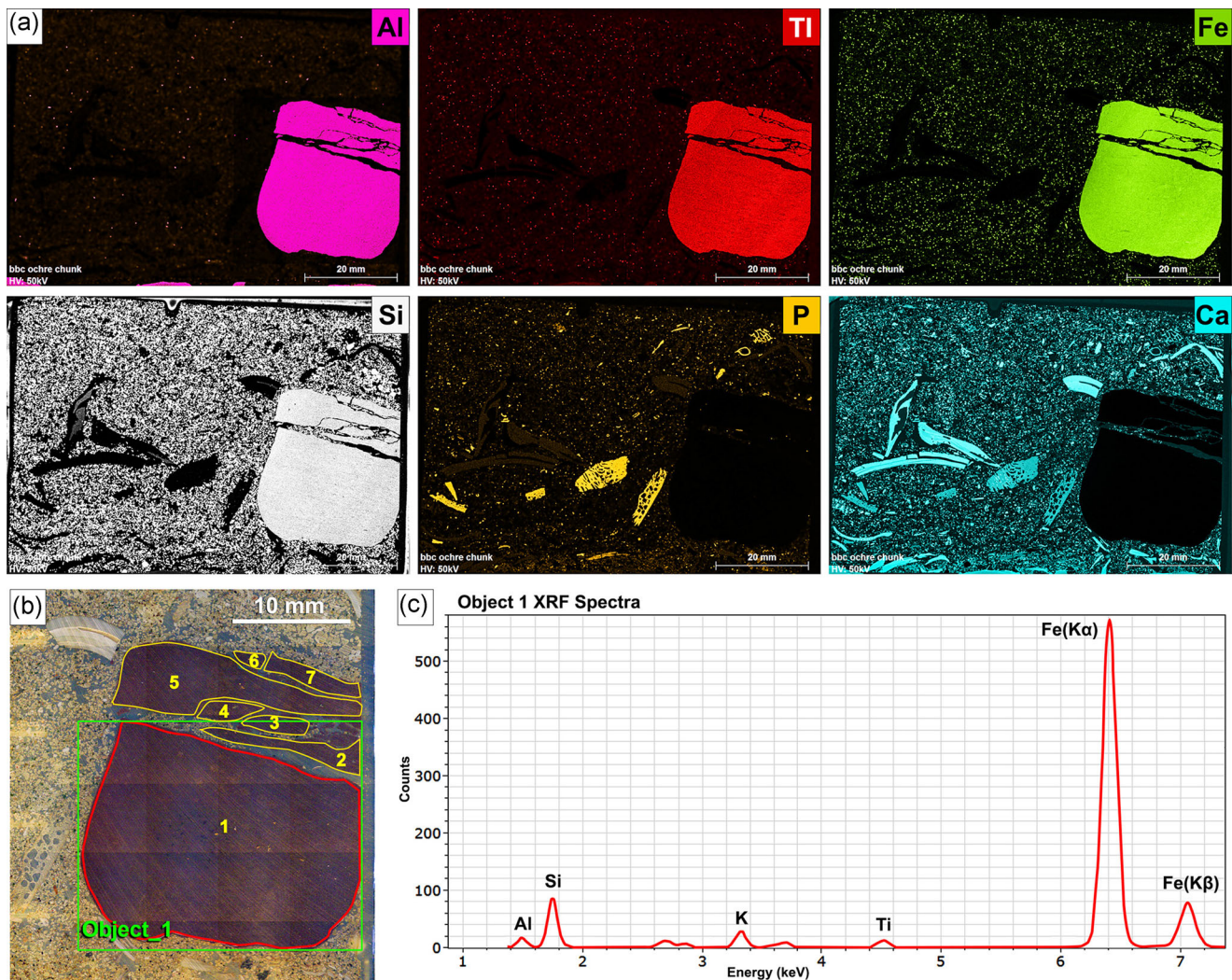


FIGURE 13 (a) Micro-X-ray fluorescence (XRF) elemental maps showing the spatial distribution of aluminium (Al), titanium (Ti), iron (Fe), silicon (Si), potassium (P) and calcium (Ca) within the thin-section BBC-13-16-A. (b) Reflected light photomicrograph of the trapped ochre within the thin sections. The yellow numbers reflect the location of the seven ochre fragments subjected to m-XRF elemental mapping. (c) Micro-XRF spectra of the area outlined in red in (b) (Fragment 1). See Table 1 for XRF overview data and Tables S2–S8 for detailed results [Color figure can be viewed at wileyonlinelibrary.com]

wall and may be laterally traced as cm-thick lenticular structures across large parts of the site, suggesting that the M2 upper was a period of frequent and recurrent cave visits (Haaland, 2018). This interpretation is reinforced by 3D reconstruction of the occupation surfaces surrounding the trapped ochre (Figure 8), which show the presences of large amounts of lithic debris, faunal remains and shellfish fragments.

In the thin section (Figures 9 and 10), the most common microfacies observed near the trapped ochre are those that contain a mix of quartz-rich calcareous sand intermixed with a variable amount of coarse and fine fraction. Due to the anthropogenic origin of the coarse fraction components (bones, shellfish, lithics and charred material), we thus relate the deposition of the ochre piece to a period of human occupation of the cave. However, the distribution, orientation, fragmentation and densities of the humanly deposited coarse fractions vary greatly.

From the close-up thin-section scans (Figure 10a), we notice that the trapped ochre piece is not directly associated with an intact cemented hearth feature just below it. Rather, the base of the ochre rests on micro-laminated occupation deposits (see “Occ I” in Figure 9d) that contain numerous fragments of chipped coarse fractions (e.g., snapped shell fragments and crushed bone). The microlaminations containing the highest concentrations of occupation debris (“Occ. I”) show more massive microstructure than the sandier laminations (“Sandy” or Occ. II–III), and the fraction within it exhibits a clear horizontal orientation and parallel distribution. In sum, these observations suggest that the occupation deposits just below the trapped ochre were affected by overlapping human surface activities, such as trampling (Rentzel et al., 2017).

The deposits in which the ochre is directly embedded (Occ. II in Figures 9d and 10b) show considerably fewer inclusions of the heavily fragmented coarse fraction. In addition, this deposit exhibits

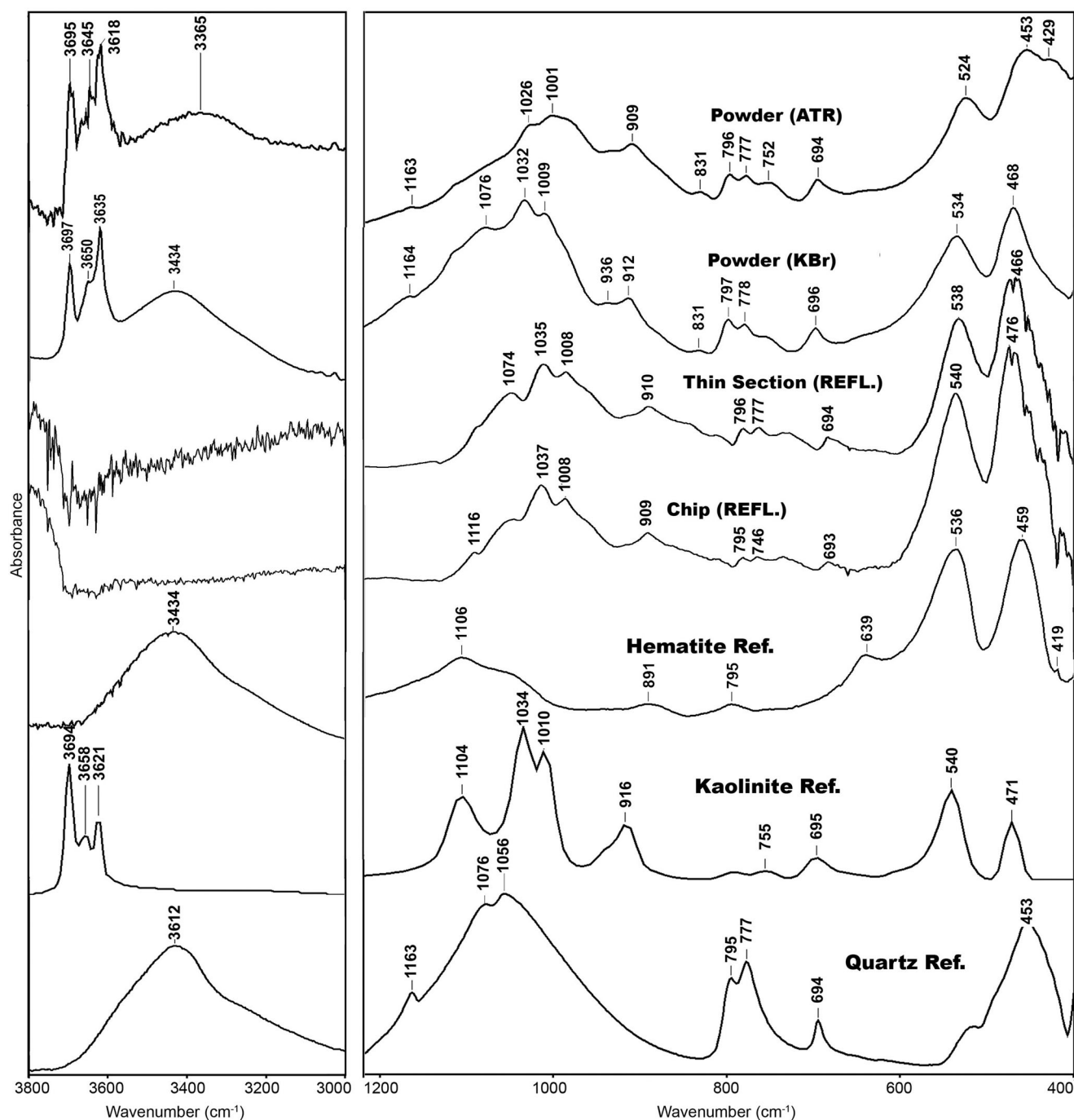


FIGURE 14 Infrared spectra of the trapped ochre piece collected in a powdered form (attenuated total reflection [ATR] and KBr transmission mode) and from its chip and thin-section surfaces (reflected mode [REFL.]). Reference (REF.) spectra of powdered Haematite (KBr; Weiner Library 2007–2009), Kaolinite and Quartz (KBr, Nicolet JHU)

a more open microstructure with no evidence for internal micro-layering. The random and nonlinear orientation of elongated shellfish and bone fragments, combined with the more open microstructure, suggests that these sediments may still have been moderately re-worked and disturbed through dumping or sweeping activities (Goldberg et al., 2009; Miller et al., 2013).

Finally, the trapped ochre piece was found in close proximity to another large ochre piece, recovered within the same layer, some

20 cm apart (Figure 8c). It is, thus, possible that both ochre pieces were in use during the same occupation event, and that both were intentionally left behind or discarded.

Unlike the dense and trampled occupation deposits that the ochre is resting on, the sedimentary matrix that surrounds and covers it contains larger and less fragmented pieces of shellfish and bone that show less sign of compaction (Figure 10b). This may indicate that the ochre piece was left at the site during an

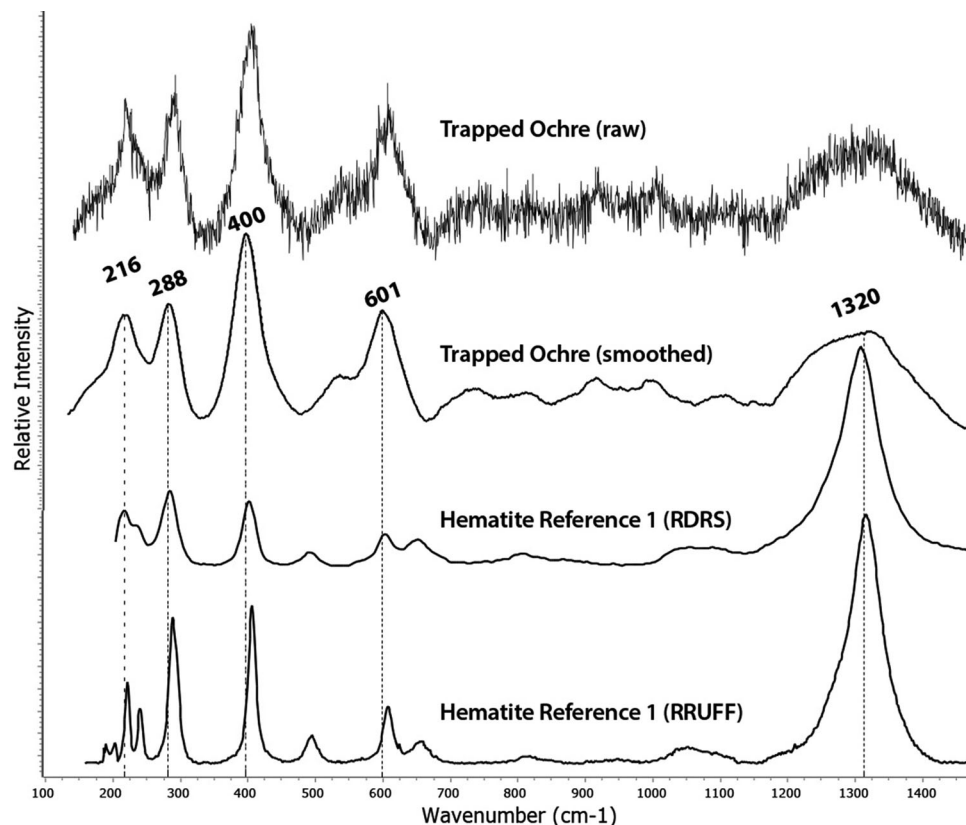


FIGURE 15 The micro-Raman spectra of the trapped ochre piece, as measured directly on the uncovered thin section, compared with the reference Raman spectra of haematite from the RRUFF project (Lafuente et al., 2016) and the RDRS project (Buzgar, 2009)

abandonment phase, during which, occupation debris was left on the surface and subjected to considerably less repeated trampling and fragmentation. This interpretation is supported by the fact that the layers (CFA and CDB) situated directly above the trapped ochre piece have previously been defined as very low-intensity occupation deposits, containing very few microscopic or macroscopic archaeological material and dominated by calcareous sand and roof spall (Haaland, 2018).

6.2 | Evaluating the mineralogical and elemental analyses

The geochemical methods employed in this paper were selected for several reasons. First, we chose methods that would yield both elemental and molecular information, as similar approaches are typically employed in conventional ochre studies (e.g., Bouillot et al., 2017; Román et al., 2019; Wojcieszak & Wadley, 2019; Zipkin et al., 2017). Second, we aimed to achieve nondestructive or minimally destructive sampling. Although this may seem counterintuitive—as one could argue that the ochre piece has already been destroyed—there is an increasing emphasis in the field of archaeological micromorphology on integrating traditional petrographic observations with other microscopic analyses conducted on the thin sections and slabs (Mentzer & Quade, 2013) (for southern African examples, see Berna et al., 2012; Haaland et al., 2017;

Larbey et al., 2019). Moreover, micromorphological blocks are valuable archives of portions of sites that no longer exist, and efforts should be made to conserve the remaining pieces.

Elemental analyses were conducted here using micro-XRF. The choice of instrument reflected its availability and spacious sample chamber that can accommodate large blocks. A scanning electron microscope equipped with an energy-dispersive X-ray detector or an electron microprobe with wavelength-dispersive X-ray detectors is also an appropriate technique for these types of samples and will produce similar information. Likewise, we selected micro-FTIR and micro-Raman for mineralogical analyses due to instrument access; micro-X-ray diffraction would also be a comparable choice.

Analyses using micro-FTIR and micro-Raman are nondestructive to the petrographic thin section and slab, and both techniques yielded suitable data on the trapped ochre piece. The lack of resin peaks in the FTIR spectra suggests that there was little penetration of the embedding medium into the ochre piece, which may help to explain the success of the Raman analyses. Micro-Raman analyses have been previously attempted on micromorphological samples (Goldberg, personal communication; Mentzer, 2011), but strong fluorescence of the resin likely explains the lack of published applications (Beyssac et al., 2002; Dupin et al., 2019). Lastly, both FTIR and Raman have been successfully employed in southern African MSA ochre studies (Dayet et al., 2013; Hodgskiss, 2012; Moyo et al., 2016), and our results are directly comparable to these studies.

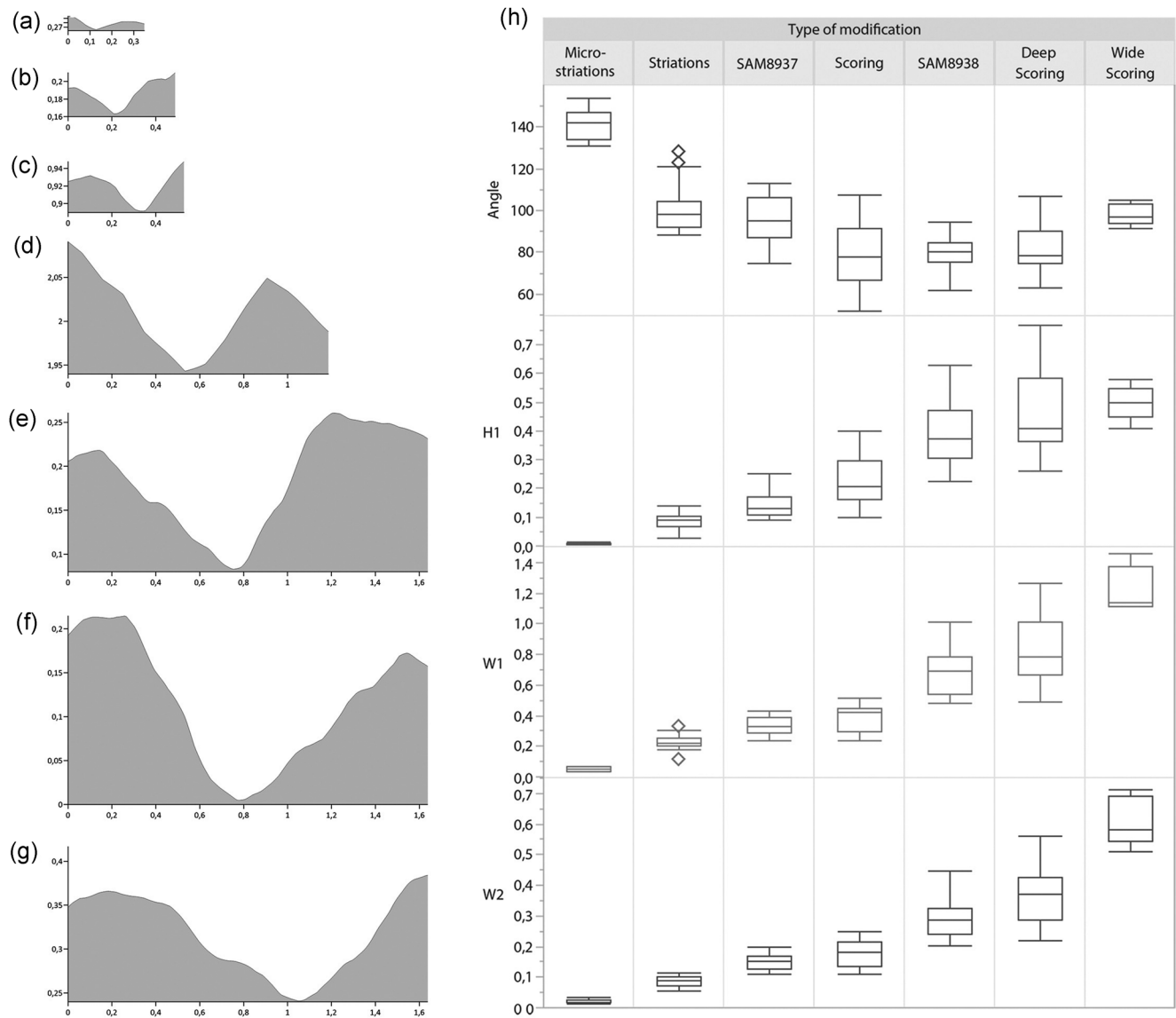


FIGURE 16 Representative profile shapes of the predefined types of ochre modifications: (a) Microstriations, (b) striations, (c) engraving (thin, SAM-AA 8937), (d) engraving (SAM-AA-8938), (e) scoring, (f) deep scoring and (g) wide scoring. Units are provided in millimetre. (h) A boxplot showing angle, maximum height (H1), maximum width (W1) and width at one-third of maximum height (W2) by the type of modification: Microstriations ($n = 11$), striations ($n = 18$), wide ($n = 5$) and deep scoring ($n = 13$), SAM 8937 ($n = 21$) and SAM 8938 ($n = 28$). It should be noted that the y-axis (i.e., the height of the profiles in (a–g) has been amplified by an elevation factor of three ($z = 3\times$) to make the profile shapes more distinguishable

There has been one previous study on Blombos ochre using analytical techniques by Moyo et al. (2016). In this study, Moyo and authors reported the most common elements found in some 68 ochre pieces detected by ED-XRF, which were Al, Si, K, Ca, Ti and Fe. This corresponds well with the elemental composition of the trapped ochre piece, which we measured through m-XRF. The lack of Mn in the trapped ochre sample is not unusual for Blombos. Whereas Mn-rich ochre artefacts have been identified, they only occur in small numbers and they do not occur consistently throughout the MSA sequence (Moyo et al., 2016). The nearby Bokkeveld shale formations (Danchin, 1970), which Moyo et al. (2016) reports may have offered sources of ochre during the MSA inhabitants of BBC, also contains low traces of Mn.

6.3 | Size, shape and physical properties

The trapped ochre (BBC-13-16-01) is one of the largest modified ochre pieces found in Blombos (Henshilwood et al., 2002; Henshilwood et al., 2009). It displays multiple flattened and faceted surfaces that are typical of intensive grinding, and the rounding of the top portion may also be the result of grinding, followed by rubbing or smoothing (Hodgskiss, 2010). The presence of these morphological features (faceting, exterior rounding) suggests that the original ochre piece had at least a medium hardness on the Mohs scale (3–4), which is the most common hardness reported from South African MSA ochre assemblages (Hodgskiss, 2013; Watts, 2002,

TABLE 3 Mean and standard deviation values of profile shape measurements by surface modification type

| | <i>n</i> | Angle | | H1 | | W1 | | W2 | |
|------------------------|----------|-------|-------|------|------|------|------|------|------|
| | | Mean | SD | Mean | SD | Mean | SD | Mean | SD |
| Wide scoring | 5 | 98.2 | 5.35 | 0.50 | 0.06 | 1.22 | 0.15 | 0.61 | 0.08 |
| Deep scoring | 13 | 81.8 | 11.15 | 0.47 | 0.15 | 0.82 | 0.23 | 0.37 | 0.10 |
| Engraving 1 (SAM 8938) | 21 | 96.6 | 11.10 | 0.14 | 0.04 | 0.34 | 0.06 | 0.15 | 0.03 |
| Scoring | 16 | 79.4 | 15.54 | 0.23 | 0.10 | 0.39 | 0.08 | 0.18 | 0.05 |
| Engraving 2 (SAM 8937) | 28 | 79.5 | 7.73 | 0.40 | 0.10 | 0.68 | 0.14 | 0.29 | 0.06 |
| Striations | 18 | 101.4 | 11.78 | 0.09 | 0.03 | 0.23 | 0.05 | 0.09 | 0.02 |
| Microstriations | 11 | 141.6 | 7.11 | 0.01 | 0.00 | 0.05 | 0.01 | 0.02 | 0.01 |

Note: Measurements were conducted on profile crosscuts with their elevation factor amplified by three times. The values in this table do not, therefore, represent absolute (real-world) values.

Abbreviations: H1, maximum height; W1, maximum width; W2, width at one-third of maximum height.

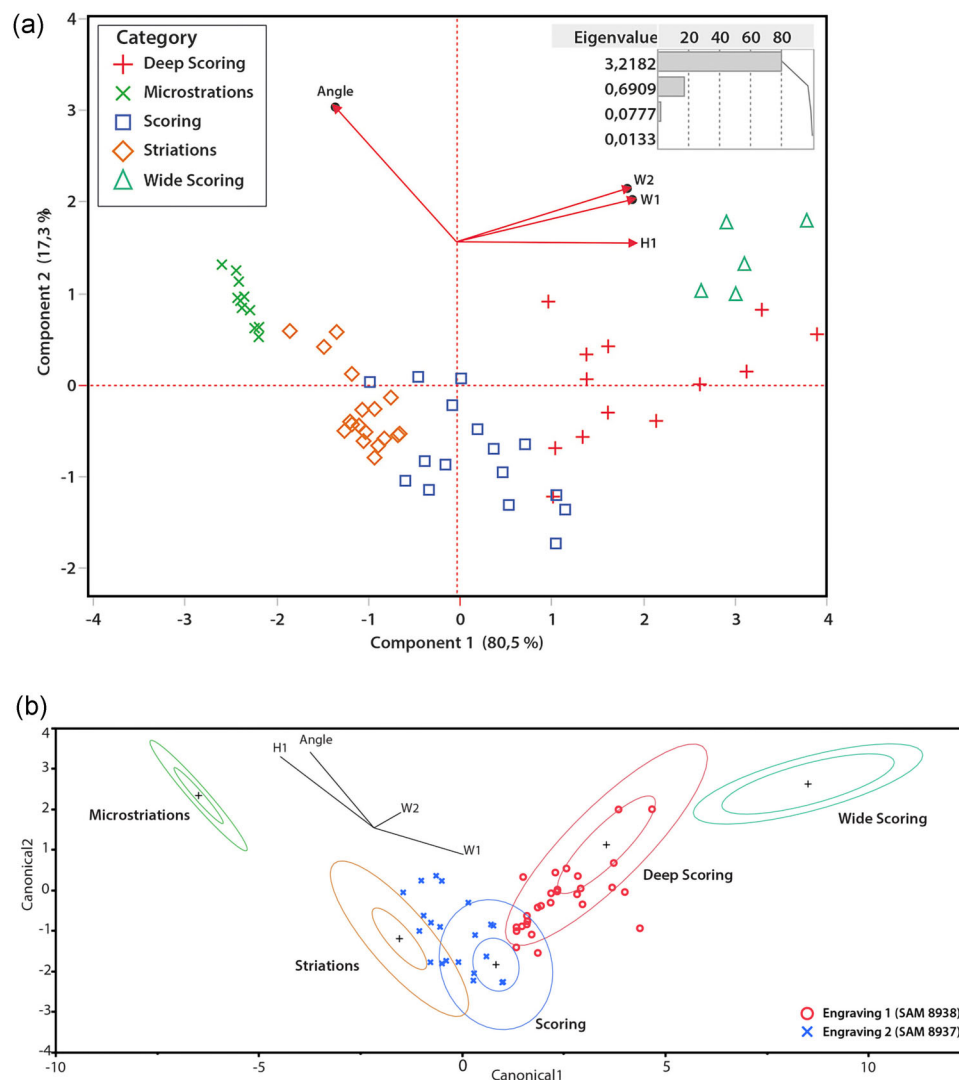


FIGURE 17 (a) Principle component analysis of profile shape measurements (angle, height and width; $n = 64$) of surface modifications on ochre by the type of modification (see Figure 15 and Table S1). (b) A canonical plot for a linear discriminant analysis of profile shape measurement (using quadratic, different covariances) showing the multivariate mean of each modification type (inner circle = 95% confidence level ellipse, outer circle = 50% class contour). Measurements of the two cross-hatched engravings are shown by blue crosses (thin engravings on SAM 8937, $n = 21$) and red circles (thicker engravings on SAM 8938, $n = 28$) [Color figure can be viewed at wileyonlinelibrary.com]

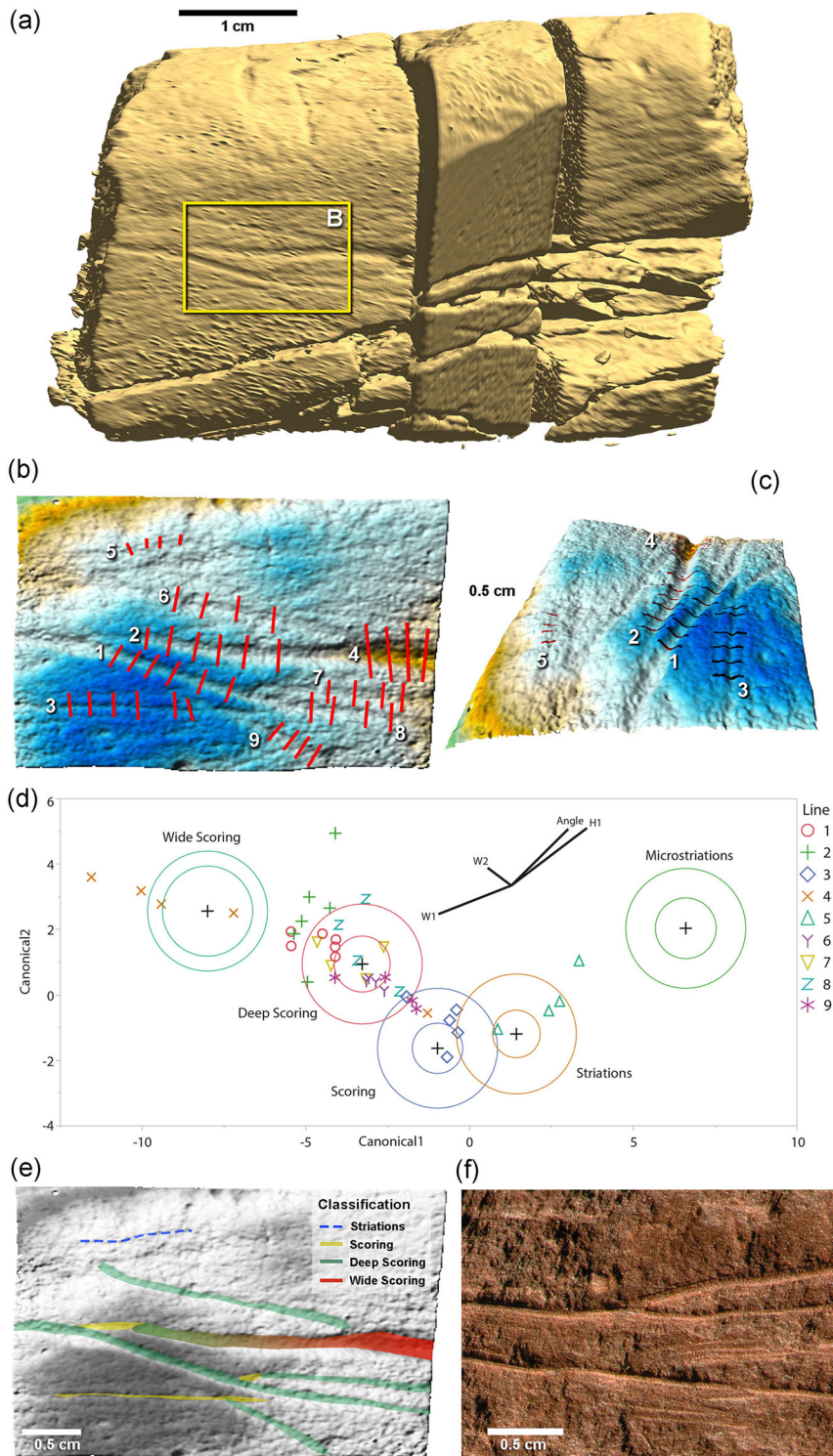


FIGURE 18 (a) Side C of the trapped ochre piece (BBC-13-16-O1). Yellow rectangle shows the surface that was selected for high-resolution three-dimensional renderings (b,c). (d) A canonical plot for a linear discriminant analysis of profile shape measurement showing the multivariate mean of each modification type (inner circle = 95% confidence level ellipse, outer circle = 50% class contour). Individual measurements conducted on the trapped ochre piece (lines 1-9) are shown by coloured symbols. (e) A visual reconstruction and classification of modification types present on Side C of the trapped ochre. (f) A photo of a modified ochre piece from the Blombos Cave Middle Stone Age ochre assemblage, comparable to the reconstructed surface (e) [Color figure can be viewed at wileyonlinelibrary.com]

2010). Ochres with a hardness ranging from 2 to 5 can produce colour streaks. As such, we may envision that the trapped ochre would have been an ideal candidate for creating pigment powder that exhibited a deep red colour (Watts, 2002), similar to numerous ochre pieces previously documented from BBC (Henshilwood et al., 2009). Combined with its homogenous fine-grained texture (Figure 12), its elemental and mineralogical composition of haematite, kaolinite and quartz (Figures 13, 14, and 15) and its fine, internal

laminations (Figure S7), the trapped ochre piece seems to represent a Fe-rich, fine-grained material, such as shale or mudstone. Both are common in the Bokkeveld Group outcrops located some 20 km from the site, and this has previously been suggested as the most likely source for many of the BBC ochres (Henshilwood et al., 2009; Watts, 2009).

The micro-CT images revealed several internal weakness planes that run internally across the entire ochre piece (Figure S4).

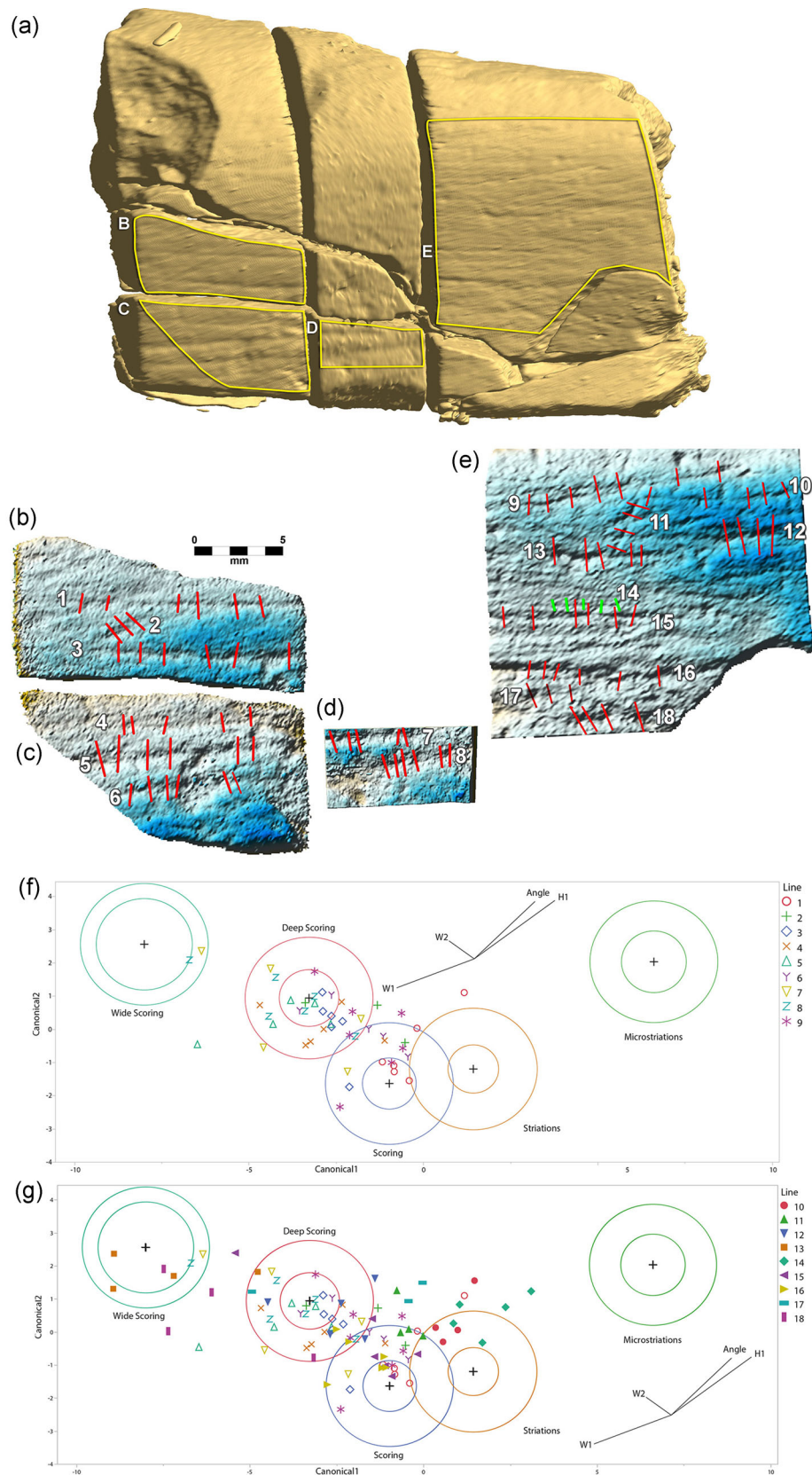


FIGURE 19 (a) Side A of the trapped ochre piece (BBC-13-16-O1). Yellow lines indicate surface areas that were selected for high-resolution three-dimensional rendering (b–e). (f,g) A canonical plot for a linear discriminant analysis of profile shape measurement showing the multivariate mean of each modification type (inner circle = 95% confidence level ellipse, outer circle = 50% class contour). Individual measurements conducted on the trapped ochre piece (Lines 1–9 [f], lines 10–18 [g]) are shown by coloured symbols [Color figure can be viewed at wileyonlinelibrary.com]

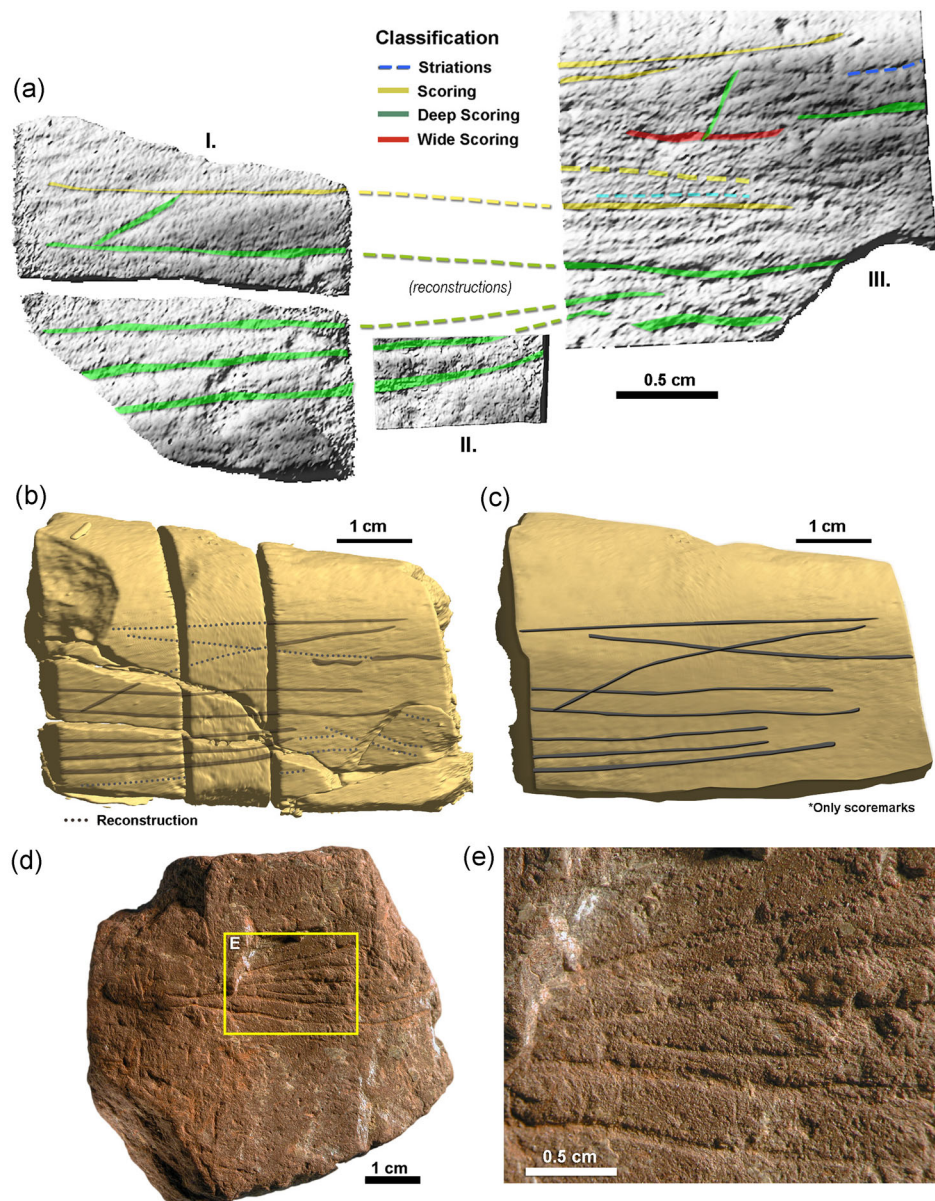


FIGURE 20 (a) A visual reconstruction and classification of modification types on the trapped ochre surface (Side A, selected surfaces). (b) An overview of the reconstructed ochre surface (Side A) with the inferred scoring and striation marks indicated. Dotted lines are likely continuation of lines. (c) A nonfragmented and uncut reconstruction of the trapped ochre piece showing the scorings marks in dark grey colour. (d,e) An overview and close-up photos of a modified ochre piece from the Blombos Cave Middle Stone Age ochre assemblage, comparable to the reconstructed surface A [Color figure can be viewed at wileyonlinelibrary.com]

The fragmentation of the ochre piece is likely related to these internal planes of weakness, but at this point, it is undeterminable whether the breakdown occurred when the ochre was deposited or buried (e.g., during tossing, dumping or sweeping actions) or whether it was induced later by postdepositional processes (e.g., trampling and compaction of the cave substrate). Micro-XRF analyses indicate that there are no enrichments or depletions of any of the measurement elements in the vicinity of the breaks, and petrographic analyses do not reveal any differences in texture or fabric near the breaks. In sum, there is no obvious geochemical explanation for why the piece is broken. We cannot rule out that the fracture also could

have occurred during the collection of the sample, but it should be noted that fractured and broken ochre artefacts are frequently encountered during excavation of the MSA layers of BBC.

6.4 | Evaluating micro-CT-based 3D reconstruction of the trapped ochre piece

In this study, several factors made the 3D reconstruction of the trapped ochre surface challenging. First, the trapped ochre was heavily fragmented. This made it time-consuming to separate the

iron-rich ochre fragments from the surrounding quartz-rich sandy matrix within the digitally reconstructed matrix. Second, the ochre piece was accidentally cut into three main slabs by the rock-saw operator during the initial processing stage, which meant that each slab had to be individually scanned and digitally processed before being aligned and made into a single model. Third, as we wanted to document even the smallest of surface marks (e.g., microstriations), the micro-CT scans were conducted at a very high resolution (the raw scanning volumes amounted to very large files of ca. 22 GB in total). To balance quality and efficiency, we used a combination of low-resolution full-scale models and high-resolution close-up views to document the occurrence, location and types of surface modifications present on the trapped ochre piece.

6.5 | Evaluating the microtopographic classification of ochre surface modifications

By using micro-CT scans of two reference ochre pieces (SAM 3937 and SAM 3938), we were able to classify the types of anthropogenic modifications present on the trapped ochre piece. The principles facilitating our classification scheme rely on two basic assumptions: (I) Different types of ochre modifications leave surface marks with different morphologies and shapes and (II) the morphometrics of different marks can be reliably measured and quantified through the microtopographic profile analysis. Although similar assumptions have been thoroughly tested and found to be correct within the anthropogenic cutmark analysis of bone (Bello & Galway-Witham, 2019; Bello & Soligo, 2008), up until now, they have not been assessed in the context of surface modifications on ochre.

The reference data set we used in this paper relied on a limited number of already known modified ochre pieces ($n = 2$). As such, these data cannot fully account for all types of anthropogenic ochre modifications. However, considering the consistent distribution patterns of morphometric measurements within the PCA and CDA plots (Figure 17), we believe our reference data set to be a reasonable representative for at least three types of generic surface modifications: Microstriations, striations and scoring. From the microtopographic comparisons of these modifications, we conclude that anthropogenic modifications of ochre surfaces are governed by physically constrained and predictable factors that indeed translate into different, redundant use-wear patterns that can be morphometrically documented and quantitatively compared.

6.6 | Anthropogenic surface modifications present on the trapped ochre and behavioural implications

The artificially flattened and faceted topography suggests that all sides were once intentionally ground, and as such the entire morphology of the trapped ochre is a product of human modification. Because of the fragmentation and the crosscuts caused by the rock saw blade, it is challenging to assess the precise location and

distribution of all types of surface modifications located on the trapped ochre. Nonetheless, two of the flattened sides (A and C on Figure 11) have distinct striation and score marks that run parallel with the elongated axis of the piece. Our 3D reconstruction and profile shape analysis show that several of these surface modifications can be classified as different types of score marks. Side A, which exhibits between five and eight parallel lines (Figure 20) can all be classified as either scorings or deep scorings, making them comparable in size and shape to cross-hatched pattern incisions on the SAM 8839 (Figure 6). Side C contains at least five scorings (-Figure 18). The score marks on both side A and C are all aligned with the general, elongated axis of the ochre piece itself, and their paths seem to cross each other randomly. On the basis of these observations, it is likely that the score marks on sides A and C of the trapped ochre were intentionally made and represent incisions produced by a sharp object.

Do the lines on Side A or Side C of the trapped ochre piece represent instances of intentional engraving, that is, some type of overarching design? According to Henshilwood et al. (2009), examples of engravings include, but are not limited to, multiple score marks that constitute a deliberately arranged pattern which would have required a specific and controlled hand motion and would, thus, have been incompatible with effective powder production. They furthermore argue that engravings typically comprise similar-sized, juxtaposed score marks that exhibit uniform cross-sections, indicating that a constant pressure was applied during the incision process of all the lines and that the lines were produced by the same tool during a single session. Following the criteria of Henshilwood et al. (2009), the variety of score marks on Side C do not qualify as engravings. The parallel lines on Side A, on the contrary, appear to be made with the same tool and pressure, they are uniformly distributed, and they appear to be deliberately aligned with each other and with the edge of the piece. Consequently, they bear a clear resemblance to previously documented engravings from BBC (Henshilwood et al., 2009), and would most likely have been defined as such if a conventional, qualitative investigation had been possible.

6.7 | A brief discussion on ochre modification terminology

Although numerous studies of African ochre assemblages focus on identifying anthropogenic use traces on ochre pieces (Bernatchez, 2012; Bouillot et al., 2017; Dayet et al., 2016, 2017; de la Peña et al., 2019; Henshilwood et al., 2002, 2009; Hodgskiss & Wadley, 2017; Hodgskiss, 2012, 2013; Rosso et al., 2017; Watts et al., 2016; Watts, 1999, 2002, 2009, 2010), there is currently no consensus on terminology for specific types of ochre modifications. Though certain terms are, in general, agreed upon (i.e., striation, crayon and scoring), in many cases, the researchers often use terms adapted to the local context and site-specific ochre assemblage. For example, both Watts (2010) and Rosso et al. (2017) noted the presence of *pitting* and *flaking* features in their respective ochre assemblages, yet pitting is

rarely noted in studies on other prehistoric assemblages. However, what Rosso et al. (2017) refer to as *pitting* (defined as percussion pits or depression produced by pounding actions), Watts refers to similar modifications as *notching*.

A study by Hodgskiss (2010) sought to rectify some of these discrepancies by identifying the specific behaviours or actions responsible for certain types of modifications seen on experimentally modified ochre pieces. Following a similar rationale, Rosso et al. (2017) explored the effect that different grindstone textures had on the coarseness of the ochre powder being produced. However, both studies focused more on linking ochre processing actions to specific types of surface modifications. Less emphasis was placed on quantitative documentation and defining the observed modifications, in terms of their 3D morphology and metric size.

Within this context, our paper may serve as a case study that demonstrates both the need and the benefits of quantitatively characterising and classifying ochre surface modifications in a standardised and consistent way. Profile shape measurements on ochre can easily be conducted on conventionally recovered pieces. Microtopographic data sets can be acquired not only through micro-CT scanning, but also through alternative methods such as confocal microscopy or microphotogrammetry. Consequently, we regard our profile shape classification scheme to function as a proof of concept that can encourage others to adopt similar documentation strategies. This will improve intersite comparisons of ochre modifications and may thus reduce confusion in terms of ambiguous terminology.

Although we acknowledge that our ochre reference samples are locally constrained within the scope of this paper, we also believe that the observations and patterns presented here should be further tested and evaluated by controlled experiments aimed towards creating a classification scheme that is both *quantitatively* defined and *behaviourally* informed. Indeed, several of the authors of this manuscript are currently involved in a more comprehensive experimental study that focuses exclusively on linking physical modification variables, for example, ochre hardness, scoring pressure and type of implement used, to their microtopographic signatures.

7 | CONCLUSION

Our main objective in this study was to reconstruct the archaeological context, texture, composition and morphology of the trapped ochre piece and to document and characterise any possible surface modifications. For these purposes, we combined 3D field documentation, micromorphology and high-resolution micro-CT scanning with microanalytical techniques applied directly on the micromorphological slab and thin sections. The results of our investigation are as follows:

- The trapped ochre piece was deposited within a moderately reworked occupation deposit of the upper M2 phase (dated to c. 74 ka), alongside other artefacts such as lithics, bone fragments and shellfish

- It was a minimum of $5.9 \times 3.2 \times 3.7$ cm in size, making it one of the largest modified MSA ochre pieces recovered from BBC
- It had a fine-grained texture and a clay and iron-rich mineralogical composition
- It was intentionally faceted on all sides, most likely due to intensive grinding
- It had multiple scoring marks, some of which qualify for the definition of *engravings*

Our results demonstrate that a block sample-based study of a trapped archaeological artefact allows for an unusually in-depth, multiscalar and multiproxy study, enabling us to assess its depositional and microcontextual archaeological setting, its morphology and microtopography, its texture and its geochemical properties at the same time. In our specific case, the micro-CT scanning also facilitated a quantitative, morphometric profile analysis that permitted us to conduct quantitative comparisons of the surface modifications on the trapped ochre with those present on reference ochres. Even though the scope of our case study is limited to a single ochre piece, this development of a quantitative classification scheme for ochre surface modifications represents a novel attempt to objectively describe, compare and classify ochre typologies that traditionally have been only qualitatively characterised.

Although ochre materials do not occur in every archaeological context, we believe that the analytical approach presented here can be adapted and applied to any number of other materials, which may occur within a micromorphological block sample, such as bones, figurines and metallic objects, to name a few. Still, we must emphasise that micromorphological block sampling should not be avoided out of the concern of accidentally collecting significant archaeological artefacts. Through careful sampling and systematic assessment of the local field context, the risk of collecting such artefacts can be significantly reduced. In the unlikely event that complete archaeological artefacts do end up in a block sample, however, our study shows that information is neither lost nor destroyed. Rather these trapped artefacts can be robustly reconstructed and innovatively documented at a high resolution and through a wide range of spatially, physically and contextually sensitive analytical methods. Ultimately, we envision that this type of multiscalar and multidisciplinary framework may prove beneficial in the study of conventional archaeological artefacts—and not just those that are trapped.

ACKNOWLEDGEMENTS

Financial support for the analysis of the block samples was provided to Magnus M. Haaland by the Meltzer Research Fund, the Travel Fund for Doctoral Fellows at the Department of Archaeology, History, Cultural Studies and Religion. André M. Strauss is funded by FAPESP (2017/16451-2). The micromorphological block sample was collected during fieldwork at Blombos Cave 2013 under the direction of Christopher S. Henshilwood, who was funded by a South African National Research Foundation Research Chair (SARChI) at the University of the Witwatersrand, South Africa, and a European Research Council Advanced Grant, TRACSYMBOLS no. 249587. The block samples and thin sections were processed by P. Kritikakis. K.

Harvati and H. Sherf at the University of Tübingen organised the micro-CT scanning of the block, and General Electric, Stuttgart, ran the micro-CT scan of the block sample. Kudakwashe Jakata at the Microfocus CT Laboratory in the Evolutionary Studies Institute at the University of the Witwatersrand ran the scan of the reference ochre pieces. Magnus M. Haaland, Karen L. van Niekerk and Christopher S. Henshilwood are now funded by the Research Council of Norway through its Centres of Excellence funding scheme, Centre for Early Sapiens Behaviour (SapienCE), project no. 262618. The micro-FTIR applied in this study was funded by a grant from the Deutsche Forschungsgemeinschaft (MI 1748/1-1) to Christopher E. Miller. The micro-Raman spectroscopy was conducted at the University of Bergen, Norway, and facilitated by I. Dumitru. Scientific editing by Sarah Sherwood. Open access funding enabled and organized by Projekt DEAL.

CONFLICT OF INTERESTS

The authors declare that there are no conflict of interests.

AUTHOR CONTRIBUTIONS

Conceptualisation, investigation, writing original draught, writing review, and editing: Elizabeth C. Velliky. *Formal analysis, methodology, software, writing original draft, writing review, and editing:* Susan M. Mentzer. *Data curation, investigation, resources, writing review, and editing:* Karen L. van Niekerk. *Data curation, funding acquisition, project administration, resources:* Christopher S. Henshilwood.

DATA AVAILABILITY STATEMENT

Data that supports the findings of this study are available in the supplementary material.

ORCID

Magnus M. Haaland  <http://orcid.org/0000-0002-3655-3120>
 André M. Strauss  <https://orcid.org/0000-0002-2336-1381>
 Elizabeth C. Velliky  <https://orcid.org/0000-0002-3019-5377>
 Karen L. van Niekerk  <https://orcid.org/0000-0003-2261-6861>
 Christopher S. Henshilwood  <https://orcid.org/0000-0002-2818-293X>

REFERENCES

- Badenhorst, S., van Niekerk, K. L., & Henshilwood, C. S. (2016). Large mammal remains from the 100 ka Middle Stone Age layers of Blombos Cave, South Africa. *The South African Archaeological Bulletin*, 71(203), 46–52.
- Barham, L. S. (2002). Systematic pigment use in the middle Pleistocene of south-central Africa. *Current Anthropology*, 43(1), 181–190.
- Bello, S. M., & Soligo, C. (2008). A new method for the quantitative analysis of cutmark micromorphology. *Journal of Archaeological Science*, 35(6), 1542–1552.
- Bello, S. M., Vervenioutou, E., Cornish, L., & Parfitt, S. A. (2011). 3-dimensional microscope analysis of bone and tooth surface modifications: Comparisons of fossil specimens and replicas. *Scanning*, 33(5), 316–324.
- Bello, S. M., de Groote, I., & Delbarre, G. (2013). Application of 3-dimensional microscopy and micro-CT scanning to the analysis of Magdalenian portable art on bone and antler. *Journal of Archaeological Science*, 40(5), 2464–2476. <https://doi.org/10.1016/j.jas.2012.12.016>
- Bello, S. M., & Galway-Witham, J. (2019). Bone taphonomy inside and out: Application of 3-dimensional microscopy, scanning electron microscopy and micro-computed tomography to the study of humanly modified faunal assemblages. *Quaternary International*, 517, 16–32.
- Berna, F., Goldberg, P., Horwitz, L. K., Brink, J., Holt, S., Bamford, M., & Chazan, M. (2012). Microstratigraphic evidence of in situ fire in the Acheulean strata of Wonderwerk Cave, Northern Cape province, South Africa. *Proceedings of the National Academy of Sciences*, 109(20), E1215–E1220. <https://doi.org/10.1073/pnas.1117620109>
- Bernatchez, J. A. (2012). *The Role of Ochre in the Development of Modern Human Behaviour: A Case Study from South Africa* (Doctoral dissertation). Arizona State University, Tempe, AZ. <https://doi.org/10.1080/0067270X.2012.752929>
- Beyssac, O., Goffé, B., Chopin, C., & Rouzaud, J. (2002). Raman spectra of carbonaceous material in metasediments: a new geothermometer. *Journal of Metamorphic Geology*, 20(9), 859–871.
- Binford, L. R. (1981). *Bones: Ancient men and modern myths*. Academic Press.
- Boschin, F., & Crezzini, J. (2012). Morphometrical analysis on cut marks using a 3D digital microscope. *International Journal of Osteoarchaeology*, 22(5), 549–562.
- Bouillot, L. D., Wurz, S., & Daniel, F. (2017). Ochre resources, behavioural complexity and regional patterns in the Howiesons Poort. *Journal of African Archaeology*, 15(1), 20–41.
- Braun, D. R., Pante, M., & Archer, W. (2016). Cut marks on bone surfaces: influences on variation in the form of traces of ancient behaviour. *Interface Focus*, 6(3), 20160006.
- Buzgar, N., Apopei, A. I., & Buzatu, A. (2009). Romanian Database of Raman Spectroscopy. Open Access Online Database. <http://rdrs.uaic.ro>
- Buzgar, N., Apopei, A. I., Buzatu, A., Diaconu, V., & Buzatu, A. (2013). The composition and source of the raw material of two stone axes of Late Bronze Age from Neamt County (Romania)—A Raman study. *Analele Stiintifice de Universitatii Al Cuza din Iasi. Sect. 2, Geologie*, 59(1), 5.
- Cornell, R. M., & Schwertmann, U. (2003). *The iron oxides: Structure, properties, reactions, occurrences and uses*. Wiley-VCH.
- Courty, M. A., Goldberg, P., & Macphail, R. (1989). *Soils and micromorphology in archaeology*. Cambridge University Press.
- Courtenay, L. A., Maté-González, M. Á., Aramendi, J., Yravedra, J., González-Aguilera, D., & Domínguez-Rodrigo, M. (2018). Testing accuracy in 2D and 3D geometric morphometric methods for cut mark identification and classification. *PeerJ*, 6, e5133.
- d'Errico, F. (2003). Archaeological evidence for the emergence of language, symbolism, and music—An alternative multidisciplinary perspective. *Journal of World Prehistory*, 17(1), 1–70.
- d'Errico, F., & Henshilwood, C. S. (2007). Additional evidence for bone technology in the southern african middle stone age. *Journal of Human Evolution*, 52(2), 142–163. <https://doi.org/10.1016/j.jhevol.2006.08.003>
- d'Errico, F., Henshilwood, C. S., Vanhaeren, M., & van Niekerk, K. (2005). Nassarius kraussianus shell beads from Blombos Cave: Evidence for symbolic behaviour in the Middle Stone Age. *Journal of Human Evolution*, 48(1), 3–24. <https://doi.org/10.1016/j.jhevol.2004.09.002>
- d'Errico, F., Vanhaeren, M., van Niekerk, K., Henshilwood, C. S., & Erasmus, R. M. (2015). Assessing the accidental versus deliberate colour modification of shell beads: A case study on perforated Nassarius kraussianus from Blombos Cave Middle Stone Age levels. *Archaeometry*, 57(1), 51–76. <https://doi.org/10.1111/arc.12072>
- Danchin, R. V. (1970). *Aspects of the geochemistry of some selected South African fine grained sediments* (Doctoral dissertation). University of Cape Town, Cape Town, South Africa.

- Dayet, L., Texier, P.-J., Daniel, F., & Porraz, G. (2013). Ochre resources from the middle stone age sequence of Diepkloof Rock Shelter, Western Cape, South Africa. *Journal of Archaeological Science*, 40(9), 3492–3505.
- Dayet, L., Bourdonnec, F.-X.I., Daniel, F., Porraz, G., & Texier, P.-J. (2016). Ochre provenance and procurement strategies during the Middle Stone Age at Diepkloof Rock Shelter, South Africa. *Archaeometry*, 58(5), 807–829. <https://doi.org/10.1111/arcm.12202>
- Dayet, L., Erasmus, R., Val, A., Feyfant, L., & Porraz, G. (2017). Beads, pigments and early Holocene ornamental traditions at Bushman Rock Shelter, South Africa. *Journal of Archaeological Science: Reports*, 13, 635–651.
- de la Peña, P., Val, A., Stratford, D. J., Colino, F., Esteban, I., Fitchett, J. M., Hodgskiss, T., Matembo, J., & Moll, R. (2019). Revisiting Mwułu's Cave: New insights into the Middle Stone Age in the southern African Savanna biome. *Archaeological and Anthropological Sciences*, 11(7), 3239–3266.
- Dupin, A., Sordoillet, D., Fréville, K., Girardclos, O., & Gauthier, E. (2019). The taphonomic characterisation of a charcoal production platform. Contribution of an innovative pair of methods: Raman analysis and micromorphology. *Journal of Archaeological Science*, 107, 87–99.
- Erlanson, J. M., Robertson, J. D., & Descantes, C. (1999). Geochemical analysis of eight red ochres from western North America. *American Antiquity*, 64(3), 517–526.
- Goldberg, P., Miller, C. E., Schiegl, S., Ligouis, B., Berna, F., Conard, N. J., & Wadley, L. (2009). Bedding, hearths, and site maintenance in the Middle Stone Age of Sibudu Cave, KwaZulu-Natal, South Africa. *Archaeological and Anthropological Sciences*, 1(2), 95–122. <https://doi.org/10.1007/s12520-009-0008-1>
- González, M. Á. M., Yravedra, J., González-Aguilera, D., Palomeque-González, J. F., & Domínguez-Rodrigo, M. (2015). Micro-photogrammetric characterization of cut marks on bones. *Journal of Archaeological Science*, 62, 128–142.
- Güth, A. (2012). Using 3D scanning in the investigation of Upper Palaeolithic engravings: First results of a pilot study. *Journal of Archaeological Science*, 39(10), 3105–3114.
- Haaland, M. M., Friesem, D. E., Miller, C. E., & Henshilwood, C. S. (2017). Heat-induced alteration of glauconitic minerals in the Middle Stone Age levels of Blombos Cave, South Africa: Implications for evaluating site structure and burning events. *Journal of Archaeological Science*, 86, 81–100. <https://doi.org/10.1016/j.jas.2017.06.008>
- Haaland, M. M. (2018). *Geoarchaeological and micro-contextual investigations of Middle Stone Age occupation deposits at Blombos Cave, South Africa*. CRISTin database (Doctoral dissertation). University of Bergen, Bergen, Norway.
- Haaland, M. M., Czechowski, M., Carpentier, F., Lejay, M., & Vandermeulen, B. (2019). Documenting archaeological thin sections in high-resolution: A comparison of methods and discussion of applications. *Geoarchaeology*, 34(1), 100–114.
- Harvati, K., Bauer, C. C., Grine, F. E., Benazzi, S., Ackermann, R. R., van Niekerk, K. L., & Henshilwood, C. S. (2015). A human deciduous molar from the Middle Stone Age (Howiesons Poort) of Klipdrift Shelter, South Africa. *Journal of Human Evolution*, 82, 190–196.
- Henshilwood, C. S., d'Errico, F., Marean, C. W., Milo, R. G., & Yates, R. (2001). An early bone tool industry from the Middle Stone Age at Blombos Cave, South Africa: Implications for the origins of modern human behaviour, symbolism and language. *Journal of Human Evolution*, 41(6), 631–678.
- Henshilwood, C. S., Sealy, J. C., Yates, R., Cruz-Urbe, K., Goldberg, P., Grine, F. E., Klein, R. G., Poggenpoel, C., van Niekerk, K., & Watts, I. (2001). Blombos Cave, Southern Cape, South Africa: Preliminary report on the 1992–1999 excavations of the Middle Stone Age levels. *Journal of Archaeological Science*, 28(4), 421–448. <https://doi.org/10.1006/jasc.2000.0638>
- Henshilwood, C. S. (2002). Emergence of Modern Human Behavior: Middle Stone Age Engravings from South Africa. *Science*, 295(5558), 1278–1280.
- Henshilwood, C. S. (2007). Fully symbolic sapiens behaviour: Innovation in the Middle Stone Age at Blombos Cave, South Africa. In P. Mellars, K. Boyle, & O. Bar-Yosef (Eds.), *Rethinking the human revolution: New behavioural and biological perspectives on the origin and dispersal of modern humans*, McDonald Institute monographs (pp. 123–132). McDonald Institute for Archaeological Research.
- Henshilwood, C. S., d'Errico, F., Vanhaeren, M., van Niekerk, K., & Jacobs, Z. (2004). Middle Stone Age shell beads from South Africa. *Science*, 304(5669), 404. <https://doi.org/10.1126/science.1095905>
- Henshilwood, C. S., d'Errico, F., & Watts, I. (2009). Engraved ochres from the Middle Stone Age levels at Blombos Cave, South Africa. *Journal of Human Evolution*, 57(1), 27–47.
- Henshilwood, C. S., d'Errico, F., van Niekerk, K. L., Coquinot, Y., Jacobs, Z., Lauritzen, S.-E., Menu, M., & Garcia-Moreno, R. (2011). A 100,000-year-old ochre-processing workshop at Blombos Cave, South Africa. *Science*, 334(6053), 219–222. <https://doi.org/10.1126/science.1211535>
- Henshilwood, C. S., d'Errico, F., van Niekerk, K. L., Dayet, L., Queffelec, A., & Pollaro, L. (2018). An abstract drawing from the 73,000-year-old levels at Blombos Cave, South Africa. *Nature*, 562(7725), 115–118.
- Hodgskiss, T. (2010). Identifying grinding, scoring and rubbing use-wear on experimental ochre pieces. *Journal of Archaeological Science*, 37(12), 3344–3358. <https://doi.org/10.1016/j.jas.2010.08.003>
- Hodgskiss, T. (2012). An investigation into the properties of the ochre from Sibudu, KwaZulu-Natal, South Africa. *Southern African Humanities*, 24(1), 99–120.
- Hodgskiss, T. (2013). Ochre use in the Middle Stone Age at Sibudu, South Africa: Grinding, rubbing, scoring and engraving. *Journal of African Archaeology*, 11(1), 75–95. <https://doi.org/10.3213/2191-5784-10232>
- Hodgskiss, T., & Wadley, L. (2017). How people used ochre at Rose Cottage Cave, South Africa: Sixty thousand years of evidence from the Middle Stone Age. *PLOS One*, 12(4), e0176317.
- Hovers, E., Ilani, S., Bar-Yosef, O., & Vandermeersch, B. (2003). An early case of color symbolism: Ochre use by modern humans in Qafzeh Cave. *Current Anthropology*, 44(4), 491–522.
- Jacobs, Z., Jones, B. G., Cawthra, H. C., Henshilwood, C. S., & Roberts, R. G. (2020). The chronological, sedimentary and environmental context for the archaeological deposits at Blombos Cave, South Africa. *Quaternary Science Reviews*, 235, 105850.
- Karkanas, P., Brown, K. S., Fisher, E. C., Jacobs, Z., & Marean, C. W. (2015). Interpreting human behavior from depositional rates and combustion features through the study of sedimentary microfacies at site Pinnacle Point 5–6, South Africa. *Journal of Human Evolution*, 85, 1–21. <https://doi.org/10.1016/j.jhevol.2015.04.006>
- Lafuente, B., Downs, R. T., Yang, H., & Stone, N. (2016). The power of databases: The RRUFF project. *Highlights in mineralogical crystallography* (pp. 1–29). Walter de Gruyter GmbH.
- Larbey, C., Mentzer, S. M., Ligouis, B., Wurz, S., & Jones, M. K. (2019). Cooked starchy food in hearths ca. 120 kya and 65 kya (MIS 5e and MIS 4) from Klasies River Cave, South Africa. *Journal of Human Evolution*, 131, 210–227.
- Lartet, E., & Christy, H. (1875). *Reliquiae Aquitanicae: Being contributions to the archaeology and palaeontology of Périgord and the adjoining provinces of Southern France: 1865-75*. Text (Vol. 1). Williams & Norgate.
- Lombard, M. (2006). Direct evidence for the use of ochre in the hafting technology of Middle Stone Age tools from Sibudu Cave. *Southern African Humanities*, 18(1), 57–67.
- Lombard, M. (2007). The gripping nature of ochre: the association of ochre with Howiesons Poort adhesives and Later Stone Age mastics from South Africa. *Journal of Human Evolution*, 53(4), 406–419.
- Marean, C. W., Goldberg, P., Avery, G., Grine, F. E., & Klein, R. G. (2000). Middle Stone Age stratigraphy and excavations at Die Kelders Cave 1 (Western Cape Province, South Africa): The 1992, 1993, and 1995

- Field Seasons. *Journal of Human Evolution*, 38(1), 7–42. <https://doi.org/10.1006/jhev.1999.0349>
- Marean, C. W., Bar-Matthews, M., Bernatchez, J., Fisher, E., Goldberg, P., Herries, A. I. R., Jacobs, Z., Jerardino, A., Karkanas, P., Minichillo, T., Nilssen, P. J., Thompson, E., Watts, I., & Williams, H. M. (2007). Early human use of marine resources and pigment in South Africa during the Middle Pleistocene. *Nature*, 449(7164), 905–908. <https://doi.org/10.1038/nature06204>
- McBrearty, S., & Tryon, C. (2006). From Acheulean to Middle Stone Age in the Kapthurin Formation, Kenya, Transitions before the transition (pp. 257–277). Springer.
- Mentzer, S. M. (2011). *Macro- and micro-scale geoarchaeology of Üçağizlı Caves I and II, Hatay, Turkey* (Unpublished dissertation). School of Anthropology, University of Arizona, Tucson, AZ.
- Mentzer, S. M., & Quade, J. (2013). Compositional and isotopic analytical methods in archaeological micromorphology. *Geoarchaeology*, 28(1), 87–97. <https://doi.org/10.1002/gea.21425>
- Miller, C. E., Goldberg, P., & Berna, F. (2013). Geoarchaeological investigations at Diepkloof Rock Shelter, Western Cape, South Africa. *Journal of Archaeological Science*, 40(9), 3432–3452. <https://doi.org/10.1016/j.jas.2013.02.014>
- Miller, C. E., Mentzer, S. M., Berthold, C., Leach, P., Ligouis, B., Tribolo, C., Parkington, J. E., & Porraz, G. (2016). Site-formation processes at Elands Bay Cave, South Africa. *Southern African Humanities*, 29, 69–128.
- Molefe, O. (2015). *Physico-chemical characterisation of African traditional cosmetics produced by the Ovahimba tribes of Northern Namibia* (Doctoral dissertation). University of Witwatersrand, Johannesburg, South Africa.
- Moyo, S., Mphuthi, D., Cukrowska, E., Henshilwood, C. S., van Niekerk, K., & Chimuka, L. (2016). Blombos Cave: Middle Stone Age ochre differentiation through FTIR, ICP OES, ED XRF and XRD. *Quaternary International*, 404(Part B), 20–29. <https://doi.org/10.1016/j.quaint.2015.09.041>
- Ngan-Tillard, D. J., & Huisman, D. J. (2017). Micro-CT scanning, In C. N. A. G. Stoops (Ed.), *Archaeological soil and sediment micromorphology* (pp. 441–449). John Wiley & Sons Ltd.
- Rifkin, R. F. (2011). Assessing the efficacy of red ochre as a prehistoric hide tanning ingredient. *Journal of African Archaeology*, 9(2), 131–158.
- Rifkin, R. F. (2012). Processing ochre in the Middle Stone Age: Testing the inference of prehistoric behaviours from actualistically derived experimental data. *Journal of Anthropological Archaeology*, 31(2), 174–195.
- Rifkin, R. F. (2015a). Ethnographic and experimental perspectives on the efficacy of ochre as a mosquito repellent. *The South African Archaeological Bulletin*, 64–75.
- Rifkin, R. F. (2015b). Ethnographic insight into the prehistoric significance of red ochre. *The Digging Stick*, 32(2), 7–10.
- Rifkin, R. F., Dayet, L., Queffelec, A., Summers, B., Lategan, M., & d'Errico, F. (2015). Evaluating the photoprotective effects of ochre on human skin by in vivo SPF assessment: Implications for human evolution, adaptation and dispersal. *PLOS One*, 10(9), e0136090. <https://doi.org/10.1371/journal.pone.0136090>
- Román, R. S., Ruiz, M. D. L., Juan-Juan, J., Bañón, C. B., Straus, L. G., & Morales, M. R. G. (2019). Sources of the ochres associated with the Lower Magdalenian “Red Lady” human burial and rock art in El Mirón Cave (Cantabria, Spain). *Journal of Archaeological Science: Reports*, 23, 265–280.
- Rosso, D. E., Martí, A. P., & d'Errico, F. (2016). Middle Stone Age ochre processing and behavioural complexity in the horn of Africa: Evidence from Porc-Epic Cave, Dire Dawa, Ethiopia. *PLOS One*, 11(11), e0164793.
- Rosso, D. E., d'Errico, F., & Queffelec, A. (2017). Patterns of change and continuity in ochre use during the late Middle Stone Age of the Horn of Africa: The Porc-Epic Cave record. *PLOS One*, 12(5), e0177298. <https://doi.org/10.1371/journal.pone.0177298>
- Shipman, P. (1981). *Life history of a fossil: An introduction to taphonomy and paleoecology*. Harvard University Press.
- Stoops. (2003). *Guidelines for analysis and description of soil and regolith thin sections*. Soil Science Society of America.
- Tribolo, C., Mercier, N., Selo, M., Valladas, H., Joron, J.-I., Reyss, J.-I., Henshilwood, C., Sealy, J., & Yates, R. (2006). TL dating of burnt lithics from Blombos Cave (South Africa): Further evidence for the antiquity of modern human behaviour. *Archaeometry*, 48(2), 341–357.
- Unhammer, O. F. (2016). *Methodological evaluation of digital photogrammetry in a Middle Stone Age cave context. A case study from Blombos Cave, South Africa* (MA Thesis). University of Bergen, Bergen, Norway.
- Vanhaeren, M., d'Errico, F., van Niekerk, K. L., Henshilwood, C. S., & Erasmus, R. M. (2013). Thinking strings: Additional evidence for personal ornament use in the Middle Stone Age at Blombos Cave, South Africa. *Journal of Human Evolution*, 64(6), 500–517. <https://doi.org/10.1016/j.jhevol.2013.02.001>
- Villa, P., Pollarolo, L., Degano, I., Birolo, L., Pasero, M., Biagioni, C., Douka, K., Vinciguerra, R., Lucejko, J. J., & Wadley, L. (2015). A milk and ochre paint mixture used 49,000 years ago at Sibudu, South Africa. *PLOS One*, 10(6), e0131273.
- Villa, P., Soressi, M., Henshilwood, C. S., & Mourre, V. (2009). The still bay points of blombos cave (South Africa). *Journal of Archaeological Science*, 38(2), 441–460.
- Villagran, X. S., Strauss, A., Alves, M., & Oliveira, R. E. (2019). Virtual micromorphology: The application of micro-CT scanning for the identification of termite mounds in archaeological sediments. *Journal of Archaeological Science: Reports*, 24, 785–795.
- Wadley, L. (2005). Ochre crayons or waste products? Replications compared with MSA ‘crayons’ from Sibudu Cave, South Africa. *Before Farming*, 2005(3), 1–12.
- Wadley, L., Williamson, B., & Lombard, M. (2004). Ochre in hafting in Middle Stone Age southern Africa: A practical role. *Antiquity*, 78(301), 661–675.
- Wallduck, R., & Bello, S. M. (2018). Cut mark micro-morphometrics associated with the stage of carcass decay: A pilot study using three-dimensional microscopy. *Journal of Archaeological Science: Reports*, 18, 174–185.
- Watts, I. (1998). *The origin of symbolic culture: the Middle Stone Age of southern Africa and Khoisan ethnography* (Doctoral dissertation). University of London, London, UK.
- Watts, I. (1999). The Origin of Symbolic Culture. In R. Dunbar, C. Knight, & C. Power (Eds.), *The evolution of culture* (pp. 113–146). Edinburgh University Press.
- Watts, I. (2002). Ochre in the Middle Stone Age of Southern Africa: Ritualised display or hide preservative? *The South African Archaeological Bulletin*, 57(175), 1–14.
- Watts, I. (2009). Red ochre, body painting, and language: Interpreting the Blombos ochre. In R. Botha & C. Knight (Eds.), *The Cradle of Language* (pp. 93–129). Oxford University Press.
- Watts, I. (2010). The pigments from Pinnacle Point Cave 13B, Western Cape, South Africa. *Journal of Human Evolution*, 59(3), 392–411.
- Watts, I., Chazan, M., & Wilkins, J. (2016). Early evidence for brilliant ritualized display: Specularite use in the Northern Cape (South Africa) between ~500 and ~300 Ka. *Current Anthropology*, 57(3), 287–310.
- Weiner, S. (2010). *Microarchaeology: Beyond the visible archaeological record*. Cambridge University Press.
- Wojcieszak, M., & Wadley, L. (2018). Raman spectroscopy and scanning electron microscopy confirm ochre residues on 71 000-year-old bifacial tools from Sibudu, South Africa. *Archaeometry*, 60(5), 1062–1076.
- Wojcieszak, M., & Wadley, L. (2019). A Raman micro-spectroscopy study of 77,000 to 71,000-year-old ochre processing tools from Sibudu, KwaZulu-Natal, South Africa. *Heritage Science*, 7(24), 1–14.

- Wolf, S., Dapschaskas, R., Velliky, E., Kandel, A. W., Floss, H., & Conard, N. J. (2018). The use of ochre and painting during the upper Paleolithic of the Swabian Jura in the context of the development of ochre use in Africa and Europe. *Open Archaeology*, 4(1), 185–205.
- Zipkin, A. M., Ambrose, S. H., Hanchar, J. M., Piccoli, P. M., Brooks, A. S., & Anthony, E. Y. (2017). Elemental fingerprinting of Kenya Rift Valley ochre deposits for provenance studies of rock art and archaeological pigments. *Quaternary International*, 430, 42–59.
- Zipkin, A. M., Wagner, M., McGrath, K., Brooks, A. S., & Lucas, P. W. (2014). An experimental study of hafting adhesives and the implications for compound tool technology. *PLOS One*, 9(11), e112560.

SUPPORTING INFORMATION

Additional Supporting Information may be found online in the supporting information tab for this article.

How to cite this article: Haaland MM, Strauss AM, Velliky EC, et al. Hidden in plain sight: A microanalytical study of a Middle Stone Age ochre piece trapped inside a micromorphological block sample. *Geoarchaeology*. 2020;1–31. <https://doi.org/10.1002/gea.21830>